Pacific Northwest
NATIONAL LABORATORY

PNNL-28657

Assessment of the Geomechanical Risks Associated with CO_2 Injection at the FutureGen 2.0 Site

Application of the State of Stress Assessment Tool (SOSAT)

April 2019

D Appriou

U.S. DEPARTMENT OF ENERGY | Prepared for the U.S. Department of Energy under Contract DE-AC05-76RL01830

DISCLAIMER

PACIFIC NORTHWEST NATIONAL LABORATORY
operated by
BATTELLE
for the
UNITED STATES DEPARTMENT OF ENERGY
under Contract DE-AC05-76RL01830

Printed in the United States of America

Available to DOE and DOE contractors from the
Office of Scientific and Technical Information,
P.O. Box 62, Oak Ridge, TN 37831-0062;
ph: (865) 576-8401
fax: (865) 576-5728
email: reports@adonis.osti.gov

Available to the public from the National Technical Information Service
5301 Shawnee Rd., Alexandria, VA 22312
ph: (800) 553-NTIS (6847)
email: orders@ntis.gov <https://www.ntis.gov/about>
Online ordering: http://www.ntis.gov

PNNL-28657

Assessment of the Geomechanical Risks Associated with CO_2 Injection at the FutureGen 2.0 Site

Application of the State of Stress Assessment Tool (SOSAT)

April 2019

D Appriou

Prepared for
the U.S. Department of Energy
under Contract DE-AC05-76RL01830

Pacific Northwest National Laboratory
Richland, Washington 99354

Summary

This report presents the results of the application of the State of Stress Assessment Tool (SOSAT) on the FutureGen 2.0 data set. SOSAT was developed as part of the National Risk Assessment Partnership (NRAP) project and provides a unique integrated framework for estimating the state of stress probability distribution at a given depth in the subsurface and evaluating the risk of induced shear and tensile failure resulting from the injection of carbon dioxide (CO_2). The approach implemented by SOSAT is based on two deterministic and widely used methods of determining the state of stress (i.e., stress polygon and one-dimensional tectonic-elastic approach). These methods have been modified using a probabilistic approach to account for uncertainties in the input parameters. The methodology proposed in SOSAT was demonstrated using the data obtained for the FutureGen 2.0 project located in the Illinois Basin. Although the FutureGen 2.0 project was suspended by the U.S. Department of Energy prior to the start of injection operations, the extensive characterization efforts undertaken at the storage site have yielded a considerable amount of valuable data about this part of the sedimentary basin.

The FutureGen 2.0 storage site was designed to accommodate the injection of 1.1 million metric tons of CO_2 per year over a 20-year period. The injection of CO_2 and the associated pressure buildup in the reservoir is expected to alter the state of stress over the course of the injection. These changes in the initial stress state may affect fault stability and potentially lead to the unintentional creation of hydraulic fractures, which could pose a leakage risk if not contained within the reservoir. Assessing these risks is critical to making informed decisions about the characterization, management of the injection operation, and monitoring of the storage site.

The data required by SOSAT for the geomechanical assessment of the FutureGen 2.0 site were identified, and the methodology proposed in SOSAT was followed to evaluate the probability of reactivating critically oriented faults or potentially creating hydraulic fractures in the reservoir. The results of the geomechanical analysis performed using the SOSAT led to the following conclusions:

1. The probability distribution of the state of stress indicates significant uncertainties in the magnitude of the maximum horizontal stress S_{Hmax}, while the minimum horizontal stress S_{hmin} is well constrained by the stress measurements conducted during the characterization efforts at the storage site. This uncertainty in the magnitude of S_{Hmax} is a common challenge and has significant implications for geomechanical risk at sites like FutureGen 2.0 where a strike-slip tectonic regime exists.
2. The probability that the Mount Simon reservoir was initially critically stressed is relatively high—25%. When the pore pressure increases to the maximum allowable pressure permitted under the Underground Injection Control Class VI regulation of the FutureGen 2.0 project, the risk of shear failure approaches a probability of 43%. These relatively high probabilities reflect the current state of information about the geomechanical conditions in this part of the Illinois Basin. For future operations in this basin this should be a high characterization priority because it could significantly lower the risk of operations.
3. Based on the maximum injection pressure allowed in the UIC Class VI, the risk of unintentional hydraulic fracturing is limited.

The risk of shear failure as determined by SOSAT is based on a very conservative approach assuming that critically oriented faults exist in the subsurface. While no faults have been formally identified at the FutureGen 2.0 site, the results obtained with SOSAT using the

FutureGen 2.0 data set highlight the importance of integrating uncertainties in critical parameters to quantify geomechanical risks in a defensible way. Should SOSAT have been available at the time the characterization activities were being planned, more characterization efforts would have been implemented to reduce the uncertainties on the magnitude of the maximum horizontal stress, and to dismiss with confidence the potential existence of a critically-oriented fault in the reservoir (e.g., 3D seismic survey).

Acknowledgments

This work was completed as part of the U.S. Department of Energy's (DOE's) National Risk Assessment Partnership (NRAP) project, which was supported by the DOE Office of Fossil Energy, Cross-Cutting Research Program. The work was performed by Pacific Northwest National Laboratory (PNNL) under DOE contract number DE-AC05-76RL01830.

The author thanks Jeff Burghardt for his guidance on numerous aspects of the underlying theory behind the state of stress assessment tool that he developed.

Acronyms and Abbreviations

bgs	below ground surface
CCS	Carbon Capture and Storage
DOE	U.S. Department of Energy
EGS	enhanced geothermal system
EPA	U.S. Environmental Protection Agency
FMI	formation micro-imager
GCS	geologic carbon storage
GS	geological storage
HF	hydraulic fracture test
HTPF	hydraulic test on pre-existing fracture
MDT	modular formation dynamics tester
MMT	million metrics tons
NRAP	National Risk Assessment Partnership
SOSAT	state of stress assessment tool
TIV	transversely isotropic vertical
UIC	Underground Injection Control
USDW	underground source of drinking water

Contents

Figures

Tables

1.0 Introduction

Pressure changes induced by CO_2 injection operations alter the state of stress at geological carbon storage (GCS) site. These changes in the pre-injection geomechanical conditions could potentially lead to formation or reactivation of fractures which could also provide pathways for CO_2 leakage or trigger induced seismicity. For these reasons, geomechanical modeling plays a critical role in risk assessment of GCS site. In this study, a state-of-stress assessment tool developed as part of the U.S. Department of Energy's (DOE's) National Risk Assessment Partnership (NRAP) was applied to a data set derived from the proposed FutureGen 2.0 carbon capture and storage project site to assess the geomechanical risks of injecting supercritical carbon dioxide into the subsurface at a hypothetical but realistic storage site.

This report is organized as follows. The remainder of Section 1 provides background information on the scope and objectives of the study, describes how the state of stress is generally determined using two common approaches, lists the parameters required in SOSAT and presents an overview of the FutureGen 2.0 project. Section 2 provides a description of the determination of each parameter required in SOSAT with the associated data supporting their determination. Section 3 presents the results obtained with SOSAT and their implication for hypothetical CO_2 injection operations at the FutureGen 2.0 site.

1.1 Scope and Objectives

Geological storage of CO_2 involves injection of supercritical CO_2 into deep reservoirs overlain by impermeable sealing formations. At a commercial-scale storage site, the injection rate and pressure need to be sufficient to inject the large mass of CO_2 captured at a given source. While the hydraulic properties of the reservoir and sealing formations are critical when siting a storage site, the success of injecting a large amount of fluid into the subsurface is also largely dependent on the existing state of stress at the given site, and the expected alteration of the stress conditions associated with CO_2 injection.

The state of stress influences several potential risks associated with fluid injection as part of the exploitation of natural resources such as hydrocarbon, geothermal energy, or CO_2 storage. Recently, the strong increase in injection-induced seismicity, such as the rise in the earthquake rate in north-central Oklahoma associated with deep wastewater injection, have received widespread attention (Walsh and Zoback 2015; Langenbruch and Zoback 2016). Because of the similarities between CO_2 injection and other subsurface activities involving fluid injection, the seismic risk associated with carbon storage operations is real and risk assessment is critical to informing any decision-making from site characterization to the determination of operational parameters. Changes in the in situ stress conditions associated with subsurface activities can cause suitably oriented faults or fractures to slip because of shear. Fractures that are oriented to maximize the possibility of slip are referred to as "critically oriented" fractures. Similarly, fractures that would require only a minor increase in fluid pressure to slip are referred to as "critically stressed" fractures. For any activities involving fluid injection, evaluation of critically stressed fractures is fundamental for understanding the placement and orientation of injecting wells, determining the main operational parameters such as the injection rate and maximum allowable injection pressure allowed, or for deploying a risk-based monitoring strategy.

Over the last three decades, several deterministic methods have been developed to estimate the magnitudes and directions of the principal stresses and are widely used for different applications. However, none of these approaches quantify uncertainties. For some engineering

applications, unquantified uncertainties are acceptable because the risks associated with incorrect estimation are limited (Burghardt 2018). For other applications, including geologic carbon storage (GCS) or enhanced geothermal systems (EGSs), geomechanical concerns are among the principal project risk factors. For CO_2-injection projects, incorrect estimations of stress tensor components leading to fault reactivation and threatening seal integrity can potentially cause property damage, public nuisance and concern, or contamination of drinking water with brine or CO_2 (Nicol et al. 2011; White and Foxall 2016; Zoback and Gorelick 2012). These drastic consequences could eventually jeopardize the viability of a project and the entire industry (Burghardt 2018).

A tool aimed at providing a simple and conservative method for estimating the stress state at a point in the subsurface was developed as part of NRAP. The SOSAT developer modified two commonly used stress estimation methods—the stress polygon approach developed by Zoback et al. (2003) and the one-dimensional (1D) tectonic-elastic approach of Thiercelin and Plumb (1994)—using a Bayesian method to account for uncertainty in some of the input parameters. The Bayesian approach is extensively described by Burghardt (2018), and is integrated in a user-friendly environment in SOSAT, in which parameters used in the stress estimation methods mentioned above can be expressed with a degree of certainty or taken as deterministic depending on the parameter. These parameters, some required and some optional, include information about the storage formation (e.g., injection depth, pore pressure), about the regional stress regime (i.e., strike-slip, reverse, normal faulting regimes), and about the elastic properties of the injection zone. Once parameters are entered in the application, SOSAT calculates the probability distribution for the state of stress. This probability distribution is then used to evaluate the probability of activating a critically oriented fault or unintentionally creating a hydraulic fracture at a specified range of pore pressures. This approach is conservative because it assumes that a critically oriented fault exists (i.e., a fault is aligned with a plane of maximum shear stress) in the storage site. Furthermore, because faults can be activated aseismically, which may pose little to no risk, making decisions based on the risk of activation is also inherently conservative.

Burghardt (2018) demonstrated the use of the comprehensive Bayesian approach from an active enhanced oil recovery/geologic carbon sequestration field in estimating in situ stress and geomechnical risk associated with fluid disposal. This study follows a similar and simplified methodology provided by SOSAT to assess the geomechanical risks associated with CO_2 injection at a realistic GCS site, the storage site initially envisioned for the FutureGen 2.0 project.

1.2 Determination of the State of Stress: Theoretical Background

At the basis of the probability distributions for in situ stress determination used in SOSAT are two deterministic stress estimation methods: the stress polygon approach (Zoback et al. 2003) and the 1D tectonic-elastic approach (Thiercelin and Plumb 1994). These approaches are widely discussed in the literature, and are briefly presented here to highlight the importance of some of the input parameters that will later be required by SOSAT.

It is often assumed that although stress is a tensor with six independent components, in most cases the greatest, intermediate, and least principal stress S_1, S_2, and S_3 are referred to as S_v, S_{Hmax} and S_{hmin}, as initially proposed in the Anderson's faulting theory (Anderson 1951; Zoback et al. 2003). The Coulomb-Navier criterion in frictional equilibrium assumes that failure is only a function of the difference between the least and the greatest principal stress S_1 and S_3. Jaeger

and Cook (1979) showed that for optimally oriented faults, the ratio of maximum to minimum effective stress at which slip will occur is given by:

$$\frac{S_1 - P_p}{S_3 - P_p} = \left[(\mu^2 + 1)^{1/2} + \mu\right]^2 \quad (1)$$

where P_p is the pore pressure and μ is the coefficient of friction.

The limiting stress differences ratio for each stress regime assuming Anderson's theory of faulting is given in Equation (1). Stated differently, for a given pore pressure P_p and coefficient of friction μ, the differential stress magnitudes cannot exceed the stress required to cause shear failure on pre-existing, optimally oriented faults (i.e., those oriented in the direction of maximum shear). The maximum difference between S_v and S_{hmin} is therefore limited by the normal faulting regime, the maximum difference between S_{Hmax} and S_{hmin} is limited by the strike-slip faulting regime, and the maximum difference between S_{Hmax} and S_v is limited by the reverse faulting regime to cause shear failure on critically oriented faults. This constitutes the stress polygon approach originally proposed by Zoback et al. (2003), illustrated in Figure 1 and summarized in Table 1.

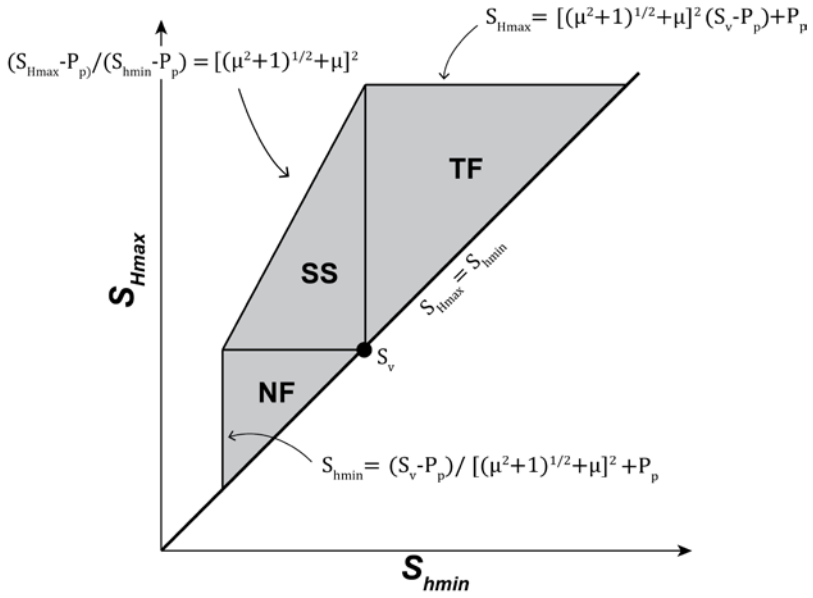

Figure 1. Illustration of the stress polygon approach used in SOSAT for the determination of in situ stress (modified from Zoback et al. 2003). Each polygon defines possible stress magnitudes for a given stress regime, where NF = normal faulting, SS = strike-slip faulting regime, and RF = reverse faulting.

Table 1. Limiting stress differences for each stress regime.

Stress Regime (Anderson's Theory)	Relative Stress Magnitude	Limiting Stress Differences
Normal Faulting (NF)	$S_v > S_{Hmax} > S_{hmin}$	$\frac{\sigma_1}{\sigma_3} = \frac{S_v - P_p}{S_{hmin} - P_p} \leq [(\mu^2 + 1)^{\frac{1}{2}} + \mu]^2$
Strike-Slip Faulting (SS)	$S_{Hmax} > S_v > S_{hmin}$	$\frac{\sigma_1}{\sigma_3} = \frac{S_{Hmax} - P_p}{S_{hmin} - P_p} \leq [(\mu^2 + 1)^{\frac{1}{2}} + \mu]^2$
Reverse Faulting (RF)	$S_{Hmax} > S_{hmin} > S_v$	$\frac{\sigma_1}{\sigma_3} = \frac{S_{Hmax} - P_p}{S_v - P_p} \leq [(\mu^2 + 1)^{\frac{1}{2}} + \mu]^2$

The second approach used to develop the probability distribution in SOSAT is the 1D tectonic-elastic model proposed by Thiercelin and Plumb (1994). This model assumed that one of the stresses is vertical, and at a depth of interest z is equal to the weight of the overlying material:

$$\mathrm{S_v} = \int_0^{\mathrm{z}} \rho(\mathrm{z}) \mathrm{g} \mathrm{dz} \tag{2}$$

The two horizontal principal stresses S_{hmin} and S_{Hmax} are then estimated by solving the linear poroelasticity equations for horizontal stresses, with vertical stress set equal to the overburden weight (Burghardt 2018; Thiercelin and Plumb 1994):

$$S_{hmin} = \frac{E_h}{E_v} \frac{v_{hh}}{1 - v_{vh}} \left(S_v - \alpha_v P_p\right) + \frac{E_h}{1 - v_{hh}^2} (\varepsilon_H + v_{hh} \varepsilon_h) + \alpha_h P_p \tag{3}$$

$$S_{Hmax} = \frac{E_h}{E_v} \frac{v_{hh}}{1 - v_{vh}} \left(S_v - \alpha_v P_p\right) + \frac{E_h}{1 - v_{hh}^2} (\varepsilon_H + v_{hh} \varepsilon_H) + \alpha_h P_p \tag{4}$$

where

E_h = horizontal Young's modulus
E_v = vertical Young's modulus
v_{hh} = horizontal-horizontal Poisson's ratio
v_{vh} = vertical-horizontal Poisson's ratio
α_h = horizontal component of the Biot coefficient tensor
α_v = vertical component of the Biot coefficient tensor
ε_H = maximum horizontal strain
ε_h = minimum horizontal strain.

Equations (3) and (4) show that the two horizontal stresses are a combination of the lateral effect of the overburden, referred to as the "Poisson effect", and the contributions of the tectonic strains to the horizontal stresses. Based on these equations, the assumption that poroelastic properties are uniform in the horizontal direction, and that for anisotropic material, the vertical direction is a direction of material symmetry, the state of stress at any given depth is then a function of the weight of the overburden, the poroelastic properties, and the horizontal strain.

As stated above, the SOSAT developer modified these two deterministic approaches to account for uncertainty in the input parameters using a Bayesian approach. The implementation of the Bayesian approach is extensively discussed by Burghardt (2018), and is not described further in this report. Any user of SOSAT is invited to refer to the Burghardt paper before using the tool in order to have a sound understanding of the importance of the choice of parameters.

1.3 Parameters Required in SOSAT

In SOSAT, most of the parameters required to assess the geomechanical risk associated with fluid injection are expressed as a probability distribution reflecting the degree of certainty with which the parameters are known, while others are expressed as deterministic parameters. The parameters required in SOSAT are listed in Table 2, along with their associated degree of certainty with which they are known, and a reminder of their main function for the evaluation of the geomechnical risk.

Table 2. List of parameters required in SOSAT, their requested degree of certainty, and their main purpose in the geomechanical risk assessment.

Parameters	Degree of Certainty	Purpose
Reservoir Properties		
Friction coefficient (mean/ standard deviation/ maximum possible)	Probability distribution (log normal distribution)	Constrain the stress difference for each faulting regime (stress polygon approach from Zoback et al. (2003)
Reservoir depth	Deterministic parameter	Analyze of the state of stress in SOSAT at this given depth (true vertical depth)
Pore pressure gradient	Deterministic parameter	Determination of state of stress
Average overburden density	Deterministic parameter	Determination of the vertical principal stress (S_v)
Maximum injection pressure	Deterministic parameter	Maximum pore pressure that will be used in the fault activation probability calculations.
Regional Stress Information		
Faulting regime weight/ faulting regime transition parameters	Probability distribution	Relative weight assigned to the three faulting regimes. Allows expression of the stress state as a probability distribution using a superposition of two logistic functions. Transition parameters control how gradual the transition between the different faulting regimes is.
Stress Measurements (optional)		
Minimum principal stress (mean/standard deviation)	Probability distribution (normal distribution)	Used to better constrain the posterior distribution of horizontal stresses
Calculation and Plot		
Number of trial stress states	Deterministic – user-defined value	Control the rejection sampling algorithm used to generate a representative sample of stress states from the posterior distribution.
Minimum and maximum values of the stress path coefficient	User-defined value	Used to create a uniform distribution for the stress path coefficient (ratio of the change in the total minimum principal stress, resulting from a change in the pore pressure). Defined using elastic properties from core measurements from the reservoir.

Parameters	Degree of Certainty	Purpose
Stress grid size	User-defined value	Control the resolution of the grid.
Minimum stress to plot	User-defined value	Control the ranges of the stresses plotted on the posterior stress distribution plot.
Number of injection pressures to evaluate	User-defined value	Control how the fault activation probability curve is plotted. Specify the number of pore pressures between the initial pore pressure and the maximum injection pressure.

1.4 Overview of the FutureGen 2.0 Project

The FutureGen 2.0 project was a DOE/private industry-funded project intended to demonstrate the effectiveness and technical feasibility of industrial-scale geological storage (GS). The project envisioned operating a commercial-scale carbon capture and storage (CCS) system capable of capturing, treating, transporting, and storing the CO_2 from a coal-fired power plant located in Meredosia, Illinois (Figure 2). The plant was designed to capture

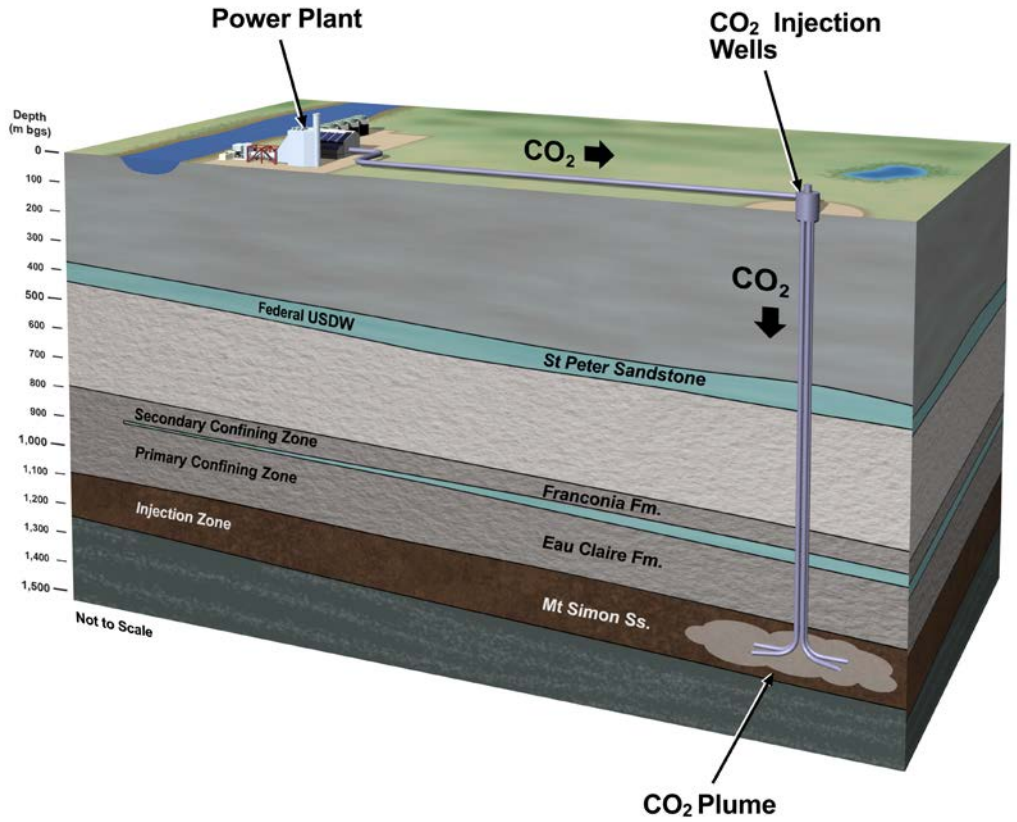

Figure 2. Conceptual design of the FutureGen 2.0 Project, Illinois, USA. CO_2 was to be captured at the Meredosia Power Plant, transported through a pipeline, and injected in the Mount Simon Sandstone.

approximately 1.1 million metrics tons (MMT) of CO_2 annually using oxy-combustion and carbon capture technology over a 20-year period. The CO_2 captured at the Meredosia Power Plant was

to be transported through a 45 km pipeline to a permanent storage site located in Morgan County, Illinois, where it would have been injected into a deep saline geological formation through four lateral injection wells.

Although DOE suspended the FutureGen2.0 project activities in January 2015, significant advances were made for nearly 5 years on the downstream component of the demonstration to site, design, construct, and operate an underground CO_2 storage reservoir with sufficient capacity to sequester permanently a total of 22 MMT of supercritical CO_2 over 20 years. The targeted storage formation was the Mount Simon Sandstone, an extensive saline reservoir located in the Illinois Basin, and one of the most significant carbon storage reservoirs in the United States (Figure 3). These activities were conducted in support of the applications for four underground injection control (UIC) permits with the purpose of ensuring the protection of overlying underground sources of drinking water (USDW) throughout and after the active life of the project. These efforts led to the issuance of the four first-ever Class VI UIC permits by the U.S. Environmental Protection Agency (EPA) in the United States.

The extensive characterization efforts conducted at the storage site, including the drilling of a stratigraphic borehole (FGA#1 stratigraphic well) and multiple subsequent characterization activities (e.g., hydrological tests, geomechanical tests) resulted in the development of a unique data set in this part of the Illinois Basin, that constitutes an excellent opportunity to demonstrate the methodology implemented in SOSAT.

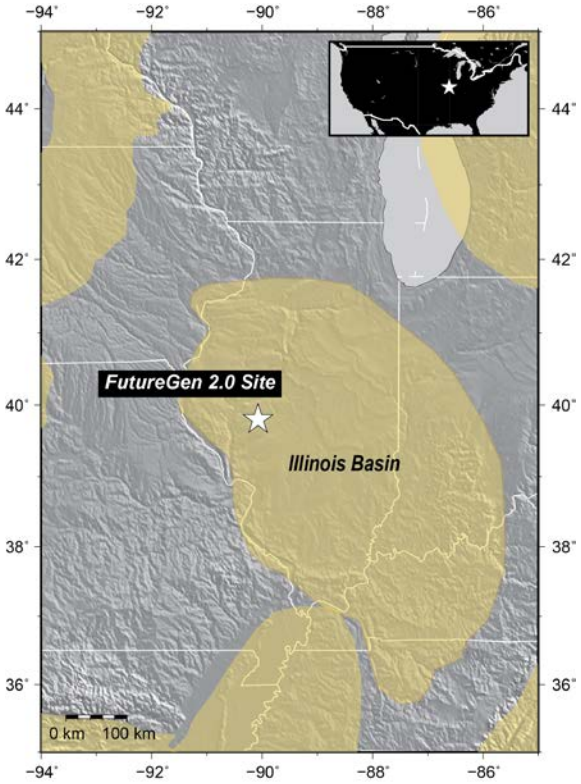

Figure 3. Location of the FutureGen 2.0 Storage Site in the Illinois Basin.

2.0 Determination of the Parameters Required in SOSAT

With the large data set collected during the characterization efforts conducted at the FutureGen 2.0 storage site, most of the parameters required in SOSAT and listed in Table 2 can be determined with a relatively well-defined degree of certainty. After a brief summary of the characterization activities performed at the FutureGen 2.0 storage site, the determination of the required parameters is discussed in detail in this section and in the order in which they are required in the current version of SOSAT.

2.1 Site Characterization Activities

A comprehensive characterization program was implemented at the FutureGen 2.0 site and formed the foundation for reducing geologic uncertainty at the storage site. As described by Gilmore et al. (2016), site characterization progressed from regional evaluation to site-specific activities, that culminated with the 2011 drilling of the FGA#1 stratigraphic borehole to a depth of 4,812 ft (1,467 m) below ground surface (bgs), which captured the entire stratigraphic sequence to the Precambrian crystalline basement rocks. The stratigraphic borehole was extensively characterized, sampled, and geophysically logged during and after drilling, generating data about geologic, hydrogeologic, or geomechanical conditions encountered at the storage site. These multiple characterization activities ranged from logging, core collection and analyses, hydrological testing and sampling, to geomechnical in situ stress determination. Details about characterization activities conducted in the FGA#1 borehole are presented in Figure 4 and Figure 5, along with the stratigraphic column.

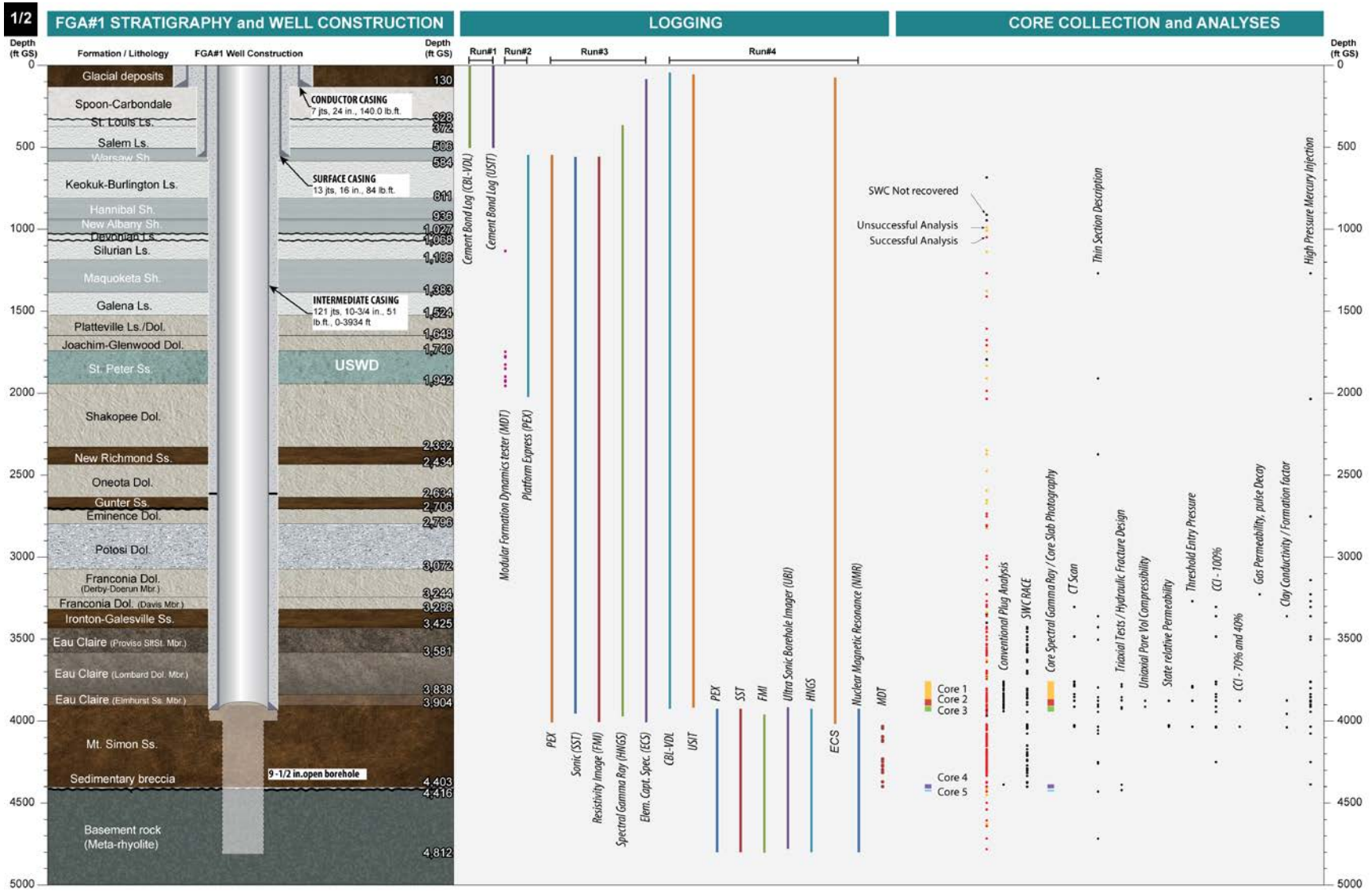

Figure 4. Summary of the characterization activities conducted in the FGA#1 borehole – logging and core collection and analysis (1/2).

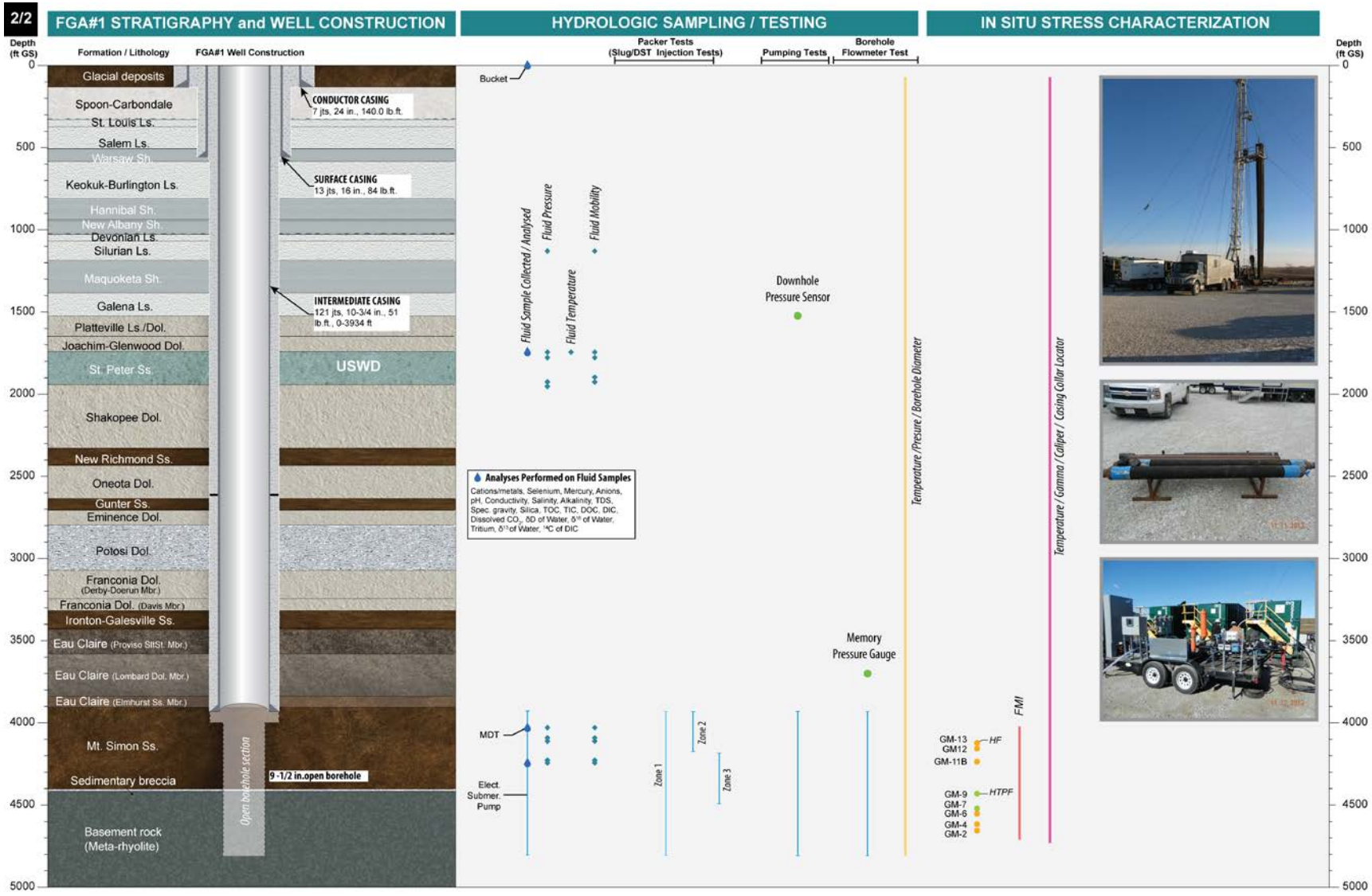

Figure 5. Summary of the characterization activities conducted in the FGA#1 borehole – hydrologic sampling/testing and in situ stress characterization (2/2).

2.2 Reservoirs Properties

2.2.1 Reservoir Depth

The Upper Cambrian Mount Simon Sandstone Formation is a major reservoir target for carbon storage that extends throughout several Midwestern states. The Mount Simon Sandstone unconformably overlies the Precambrian basement rocks, or the Pre-Mount Simon sandstones and was deposited in and on the flanks of the Proto-Illinois Basin. Regionally, the thickness of the Mount Simon Sandstone is highly variable in the basin, ranging from less than 300 ft thick in the southern Illinois Basin to over 2,000 ft thick in the northern part.

At the proposed injection location, the Mount Simon Sandstone is encountered between the depth of 3,904 and 4,416 ft (1,190 to 1,346 m) bgs in the FGA#1 stratigraphic well. The Mount Simon Sandstone is overlain by a 479 ft-thick (156 m) Eau Claire Formation, which acts as the primary sealing formation, preventing CO_2 from migrating upward. The Mount Simon Sandstone directly overlies the Precambrian crystalline basement, which is made of meta-rhyolite.

The CO_2 captured at the Meredosia Power Plant was intended to be injected through four lateral wells at a depth of about 4,030 ft (1,228 m) bgs, where a high permeability and high porosity zone (up to 23%) was identified (Figure 6). The top of the injection interval (4,030 ft) constitutes the point of reference for the geomechanical analysis conducted in SOSAT.

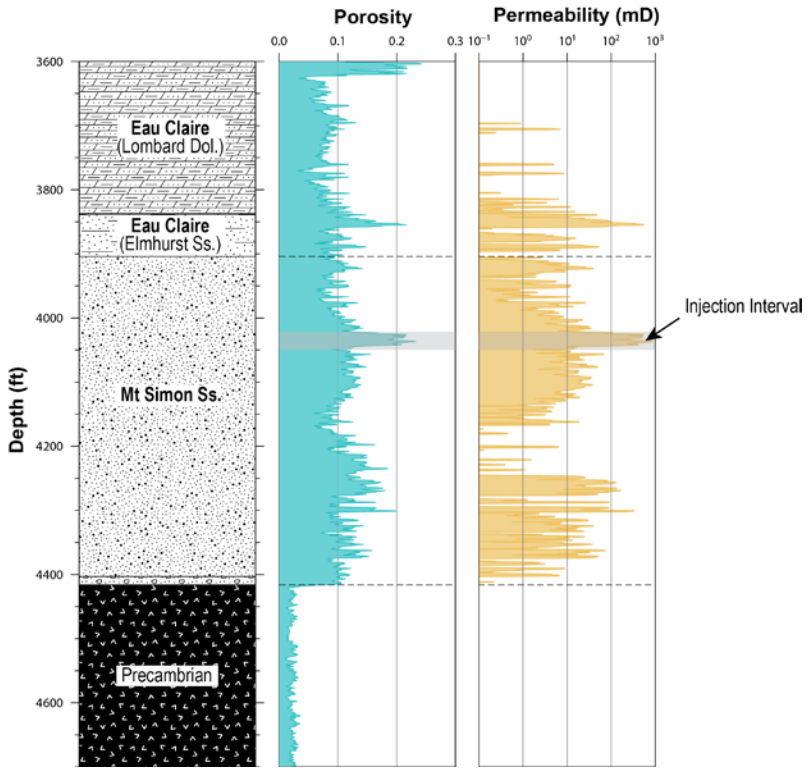

Figure 6. Porosity and permeability logs with general lithology found in the FGA#1 stratigraphic borehole at depths ranging from 3,600 to 4,800 ft (1,097 to 1,463 m) bgs. The injection interval (location of injection wells) is highlighted in gray (the top of the injection interval is at 4,030 ft).

2.2.2 Fault Friction Parameters

In SOSAT, information related to the fault friction coefficient is provided with the parameters defining a lognormal distribution (i.e., median fault friction coefficient and standard deviation). These parameters are needed because the frictional properties of these planes of weakness will constrain the possible states of stress (see Equation (1).

As explained by Burghardt (2018), it is generally not feasible to collect the frictional properties of specific faults and fractures present at a given site. However, frictional properties have been measured in laboratory and field studies and have shown that coefficients of friction between 0.6 and 1.0 (Jaeger and Cook 1979) were applicable to the crust, although typical values generally range from 0.6 to 0.7.

For the FutureGen 2.0 case study, a lognormal distribution with a mean μ_0 of 0.7 and standard deviation σ_μ of 0.15 was chosen (Figure 7). These correspond to the default parameters proposed in SOSAT.

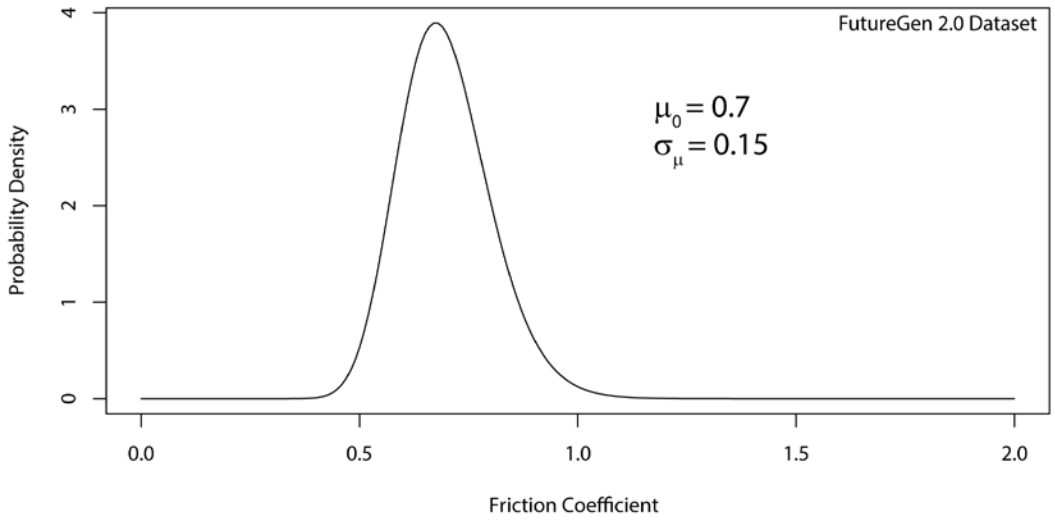

Figure 7. Lognormal probability density distribution for friction coefficient having a mean of 0.7 (μ_0) and a standard deviation of 0.15 (σ_μ).

2.2.3 Pore Pressure Gradient

Pore pressure measurements were obtained using the following three different field test characterization methods in the stratigraphic well (FGA#1):

1. Fluid samples were obtained from discrete-depth intervals using the Schlumberger Modular formation dynamics tester (MDT) tool during the process of drilling the stratigraphic well (FGA#1 well). This MDT tool has also been used to obtain measurements of reservoir pressure. Pressure data were obtained at 7 of 20 attempted sampling points in the St. Peter Formation (USDW), and at 7 of the 23 attempted sampling points in the Mount Simon Sandstone Formation.
2. Equilibrated static pressure measurements were obtained for two large Mount Simon test intervals that were isolated and hydraulically characterized using a downhole straddle packer/test system.

3. Static pressure measurements were also obtained for three 6 ft Mount Simon test/depth intervals prior to conducting geomechanical characterization tests for in situ stress determination.

Representative static pressure measurements were then obtained for the Silurian limestone (2 measurements), St. Peter Sandstone (4 measurements), and Mount Simon Sandstone (13 measurements). Pore pressure data are compiled in Table 3 and the data obtained in the Mount Simon Formation are plotted in Figure 8 .

Table 3. Representative pore pressure measurements within the FutureGen 2.0 stratigraphic well (FGA#1)

Depth (ft bgs)	Pressure (psi)	Formation	Method[(a)]	Pore Pressure Gradient
1,134.03	455.8	Silurian Ls	MDT	0.4019
1,134.97	456.06	Silurian_Ls	MDT	0.4018
1,930.99	786.9	St. Peter Ss	MDT	0.4075
1,930.06	784.34	St. Peter Ss	MDT	0.4064
1,781.99	718.16	St. Peter Ss	MDT	0.4030
1,748.96	703.39	St. Peter Ss	MDT	0.4022
4,034.01	1,775.56	Mt. Simon Ss	MDT	0.4401
4,033.95	1,775.48	Mt. Simon Ss	MDT	0.4401
4,096.48	1,803.62	Mt. Simon Ss	MDT	0.4403
4,116.02	1,812.85	Mt. Simon Ss	MDT	0.4404
4,117.00	1,813.04	Mt. Simon Ss	MDT	0.4404
3,898.44	1,708.33	Mt. Simon Ss	SP	0.4382
4,192.96	1,846.98	Mt. Simon Ss	SP	0.4405
4,235.24	1,864.1	Mt. Simon Ss	GM	0.4400
4,155.24	1,829.00	Mt. Simon Ss	GM	0.4440
4,121.55	1,815.6	Mt. Simon Ss	GM	0.4460

(a) MDT = modular formation dynamics tester, SP = straddle packer, and GM = geomechanical test.

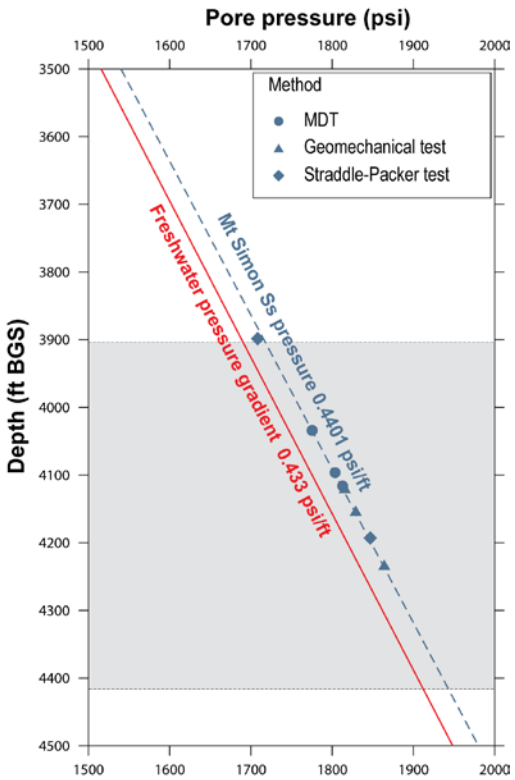

Figure 8. Mount Simon Sandstone pressure/depth measurements with freshwater hydrostatic pressure gradient and calculated Mount Simon pore pressure gradient (0.4401 psi/ft)

The average Mount Simon Formation hydrostatic pressure gradient is 0.4401 psi/ft, which is slightly higher than normal freshwater hydrostatic conditions but consistent with a calculated hydrostatic pressure gradient (0.448 psi/ft) for a fluid having the salinity of the Mount Simon fluid obtained from the FGA #1 stratigraphic well. Using the pore pressure gradient derived from measurement, the predicted fluid pressure in the injection interval (4,030 ft bgs) is 1,773.603 psi (12.25 MPa).

2.2.4 Overburden Density and Vertical Stress Determination

SOSAT requires the average overburden density as an input parameter, which is used to determine the magnitude of the vertical stress as a function of depth (Table 2). Similar to multiple approaches used to build geomechanical models, it is assumed in this approach that one of the principal stresses is vertical such that the magnitude of the vertical stress S_v is determined as the weight of the overburden material given by:

$$S_v = \int_0^{z_0} \rho g dz \quad (5)$$

where z_0 is the depth of interest, ρ is the density, and g is the gravity acceleration.

Data from density logs collected in the FGA#1 borehole are available from 566 to 4,786 ft (172 to 1,459 m) bgs. Between 0 and 566 ft (0 and 172 m) bgs, a linear gradient ranging from 2.3 to 2.4 g/cm^3 was assumed. Based on the density log, the average overburden density above the injection interval is 2.58 g/cm^3 (Figure 9). Although the vertical stress is directly computed in SOSAT, we determined and plotted the vertical stress profile by integrating the density log

throughout the entire well, leading to a vertical stress gradient 1.12 psi/ft (25.27 MPa/km) (Figure 9). The values are taken as deterministic in SOSAT.

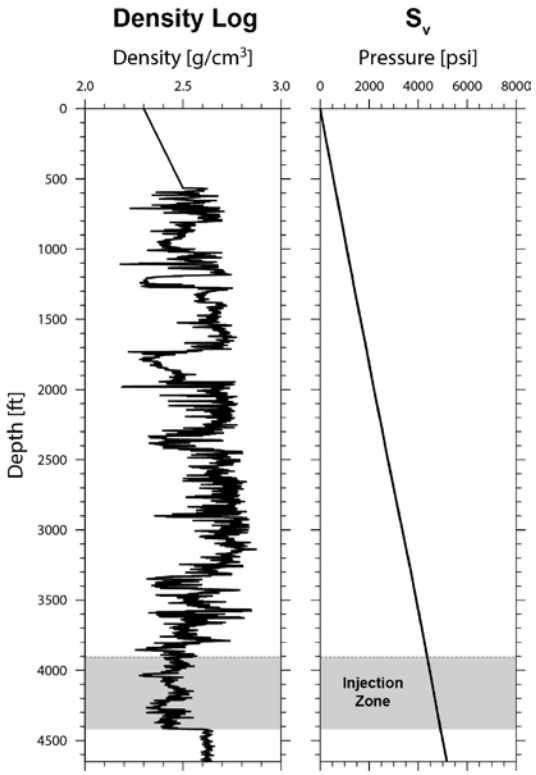

Figure 9. Density log (left) and vertical stress profile (Sv) (right) calculated by integrating the density log from the FGA#1 borehole. The average density above the injection interval (4,030 ft) is 2.58 g/cm^3.

2.2.5 Maximum Injection Pressure

The maximum injection pressure is used in the fault activation probability calculations. As part of the FutureGen 2.0 project, the maximum pressure was calculated as 90% of the fracture pressure of the injection to meet the UIC Class VI requirements. The Federal Requirements under the Underground Injection Control Program for Carbon Dioxide Geologic Sequestration Wells (75 FR 77230, December 10, 2010), referred to as the Class VI Rule, requires that injection pressure not exceed 90% of the fracture pressure of the injection zone(s) to ensure that CO_2 injection does not initiate new fractures or propagate existing ones [40CFR §146.88(a)]. At the time the UIC Class VI permit application was submitted, no geomechanical testing had been conducted and a pressure gradient of 0.65 psi/ft in the Mount Simon Formation supported by literature review was suggested to model the injection zone fracture gradient. A maximum bottom-hole injection pressure P_{max} was then determined based on the following equation:

$$P_{max} = 0.65 * 0.9 * z_{inj} \quad (6)$$

where z_{inj} the injection depth.

Once applied to the targeted injection depth (4,030 ft), the maximum pressure allowed is 2,358 psi (16.23 MPa). This value was one of the main operational parameters determined for the FutureGen 2.0 project.

2.2.6 SOSAT Inputs: Summary of Reservoir Properties

Based on the site-specific data acquired at the FutureGen site, a summary of the reservoir parameters used in SOSAT is presented in Table 4.

Table 4. Summary of the reservoir properties input parameters for SOSAT.

Parameters	Values
Median Friction Coefficient	0.7 (default)
Standard deviation of logarithm of fault friction coefficient	0.15 (default)
Maximum possible friction coefficient	1.5 (default)
Reservoir depth	4,030 feet *(1228 m)*
Pore pressure gradient	0.4401 psi/ft *(0.009955 MPa/m)*
Average overburden density	2.5 g/cm^3
Maximum injection pressure	2,358 psi *(16.23 MPa)*

2.3 In Situ Stress Measurements and Regional Stress Observations

As part of the characterization activities implemented at the FutureGen site, a geomechanical field testing program, initially meant to be the first phase of the geomechanical characterization of the storage site, was conducted before the project was shut down, preventing the project team from obtaining additional data, including stress characterization of the Eau Claire Formation, the primary sealing formation. The in situ stress measurements collected in the Mount Simon Sandstone and the Precambrian basement constitute a unique data set in this part of the Illinois Basin and provide constraints on both the stress magnitude and expected faulting regime that can be used as input parameters in SOSAT. A Phase 2 was originally planned to determine the minimum principal stress S_{hmin} in the Eau Claire caprock, and refine the potential for shear failure within the Mount Simon Sandstone and the injection interval itself. The main results obtained for the in situ stress measurements are presented and compared to regional observations below.

2.3.1 In Situ Stress Measurements

The geomechanical field testing program conducted at the FutureGen 2.0 site involved a combination of hydraulic fracture (HF) tests, often referred to as minifrac, and hydraulic tests on pre-existing fractures (HTPFs) that were performed within the open-borehole section of the FGA#1 borehole (Figure 4). Detailed testing procedures and theory for both geomechanical tests are presented by Haimson and Cornet (2003) and are not discussed further here. While the main results obtained during this first phase of geomechanical tests are presented, the complete details of the test results can be found in a technical report by Cornet (2014).

The HF method is known to yield an estimate of the magnitude and direction (with subsequent image logging) of the minimum principal stress. The HTPF method provides an evaluation of the complete stress tensor, independent of borehole orientation and material properties. Both

methods are usually recommended for optimum results (Haimson and Cornet 2003) and were implemented at the FutureGen 2.0 site as part of the characterization activities.

The field testing program included three HF tests that were conducted in the Mount Simon Sandstone and a combination of three HF tests and two HTPF tests that were performed in the underlying crystalline basement formation (Figure 10). The tests were conducted using a straddle packer to isolate the test intervals in the open section of the borehole.

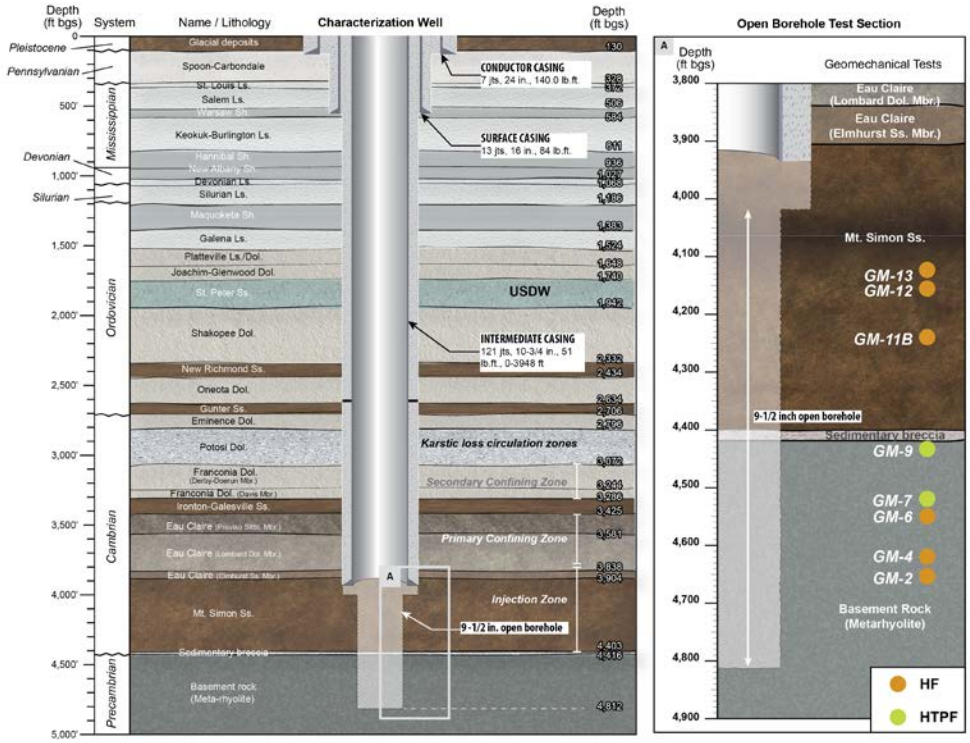

Figure 10. Location and type of geomechanical tests conducted in the open-borehole section of the FGA#1 borehole. Three geomechanical tests were conducted in the Mount Simon (HF tests) and five in the Precambrian Basement (2 HF tests and 3 HTPF tests).

2.3.1.1 Principal Stress Directions

Two of the three tests performed in the Mount Simon Formation (GM11B and GM13) exhibited distinctly vertically oriented hydraulic fractures that were created when conducting the HF tests (Figure 11). The absence of a distinctly observed fracture image for one of the tests (GM12) was only due to the sub-vertical blind area of the formation micro-imager (FMI) system. Based on this observation, it was deduced that within the Mount Simon Sandstone, the vertical direction is a principal stress direction, and that the maximum horizontal stress S_{Hmax} is oriented N51±4°E, as determined by a comparison of electrical borehole wall imaging logs (FMI logs) acquired before and after geomechanical testing.

Within the underlying Precambrian basement, images of hydraulic fractures exhibited more complexity because of interaction with pre-existing fractures. For three of the tested intervals, a consistent N63±9°E orientation of the maximum horizontal stress was obtained, while two other

tests indicated a N77°E orientation. This difference in S_{Hmax} direction suggests the existence of a local, small-scale, stress heterogeneities within the Precambrian basement.

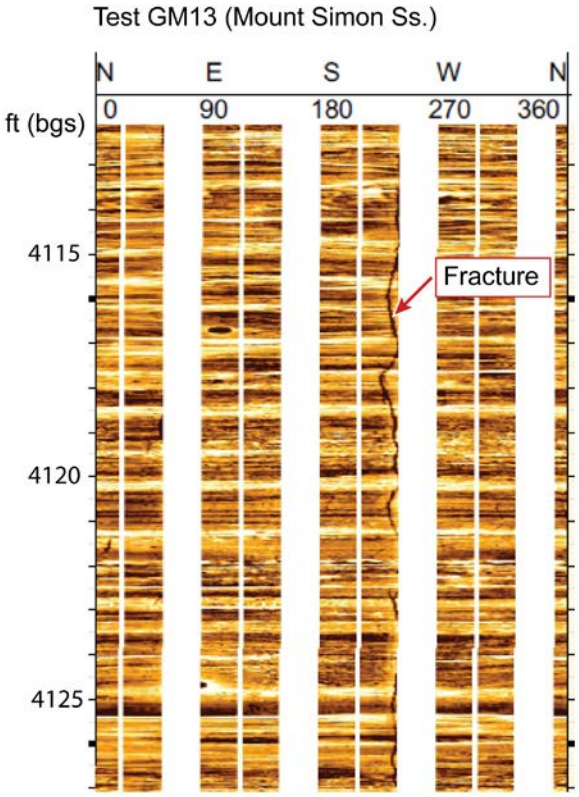

Figure 11. FMI log response following Mount Simon test GM13. The vertically oriented fracture is visible.

2.3.1.2 Vertical Principal Stress Magnitude

For the geomechanical tests, it was assumed that the vertical gradient of the vertical stress component S_v is equal to 1.071 psi/ft (0.025 MPa/m). This assumption yields values that differ only by ~2% from values estimated from wireline density measurements describved above. Experience has shown that in sedimentary formations, lateral variations are often larger than errors caused by the assumption that the vertical gradient of the vertical stress component is constant (Cornet and Röckel 2012).

2.3.1.3 Minimum Horizontal Principal Stress Magnitude

The HF tests conducted in the Mount Simon Sandstone showed that the minimum horizontal principal stress S_{hmin} does not vary linearly with depth. Two reliable estimates were obtained, namely:

$$S_{hmin} = 3240 \pm 330\, psi \;\; (22.3 \pm 2.3 \text{ MPa}) \text{ at } 4{,}156 \text{ ft } (1{,}267 \text{ m}) \text{ for test GM12} \quad (7)$$

$$S_{hmin} = 2800 \pm 100\, psi \;\; (19.3 \pm 0.7 \text{ MPa}) \text{at } 4{,}236 \text{ ft } (1{,}291 \text{ m}) \text{ for test GM11B} \quad (8)$$

Such nonlinear S_{hmin} variations with depth are likely attributable to local variations in mechanical properties and are common in sedimentary formations where the rock lithology changes in the

vertical direction. Generally, sedimentary rocks are not isotropic and exhibit anisotropic properties, including elastic properties such as Young's modulus and Poisson's ratio.

In the Precambrian basement, the three measurements conducted between 4,616 ft and 4,521 ft (1,407 m to 1,378 m) bgs (i.e., GM4, GM6, and GM7) exhibit results consistent with a local linear increase with depth:

$$S_{hmin} = 3{,}840 + 0.937(z - 4{,}521) \quad (9)$$

Note that in this equation, the stress magnitude is expressed in psi, and the depth in feet.

Based on these results, the vertical gradient of the minimum horizontal principal stress is slightly smaller than the vertical gradient of the vertical stress component. This implies that the minimum principal stress component is likely to remain in the horizontal plane at greater depths (i.e., $S_{hmin} < S_v$).

2.3.1.4 Maximum Horizontal Principal Stress Magnitude

Because HTPFs were unsuccessful in opening up pre-existing fractures in the tested intervals, the only characterization information that constrains the maximum horizontal principal stress value, S_{Hmax}, (i.e., both in the Mount Simon Sandstone and in the Precambrian basement), is the initial fracture breakdown pressure, chosen to be the packer pressure P_{pr}. The bounds for the maximum horizontal principal stress are described by the following equation:

$$3S_{hmin} - P_{pr} - P_0 + \sigma^T < S_{Hmax} < 3\,S_{hmin} - Ppr + \sigma^T \quad (10)$$

where σ^T is the tensile strength and P_0 is the far-field pore pressure.

In the absence of direct measurements for the tensile strength at the time the tests were conducted, a value of about 750 psi was adopted as a conservative underestimate for the sandstone, and 1,500 psi for the meta-rhyolite of the Precambrian basement (Cornet 2014). As a result of the tensile strength values, the maximum horizontal principal stress S_{Hmax} was consistently observed to be larger than the calculated vertical stress component S_v. This established stress relationship $S_{Hmax} > S_v > S_{hmin}$, commonly referred to as a strike-slip faulting tectonic mechanism (see section 1.2), describes the failure mechanism most likely to occur if the local pore pressure conditions become excessive.

The results of the geomechanical tests presented above are summarized in Table 5 and the vertical profiles of the three principal stresses are plotted together with the pore pressure gradient in Figure 12.

Table 5. Compilation of the results of the geomechanical test performed in the FGA#1 borehole. λ_H and γ_H are respectively the magnitude and inclination of S_{Hmax}.

Test ID	Depth (ft)	Geologic Formation	S_{hmin} (psi)	S_{hmin}/ depth	S_v (psi)	S_{Hmax} (psi)	λ_H	γ_H
GM13 (HF)	4,122	MS	*Not reliable*	-	-	*Not reliable*	N51° E	90°
GM12 (HF)	4,156	MS	3,240 ± 330	0.78±0.08	4,453	4,296 + σ^T < S_{Hmax} <6,125 +σ^T 5,046 < S_{Hmax} <6,875	N48° E	-

Test ID	Depth (ft)	Geologic Formation	S_{hmin} (psi)	S_{hmin}/ depth	S_v (psi)	S_{Hmax} (psi)	λ_H	γ_H
GM11B (HF)	4,236	MS	2,800 ± 100	0.66±0.02	4.538	$3,506 + \sigma^T < S_{Hmax} < 5,370 + \sigma^T$ $4,256 < S_{Hmax} < 6,120$	N54° E	90°
GM9 (HTPF)	4,431	Precambrian	3,645	0.82	4,747	-	N77° E	90°
GM7 (HTPF)	4,521	Precambrian	3,841	0.85	4,843	-	N62° E	90°
GM6 (HF)	4,552	Precambrian	3,897	0.86		$4,688 + \sigma^T < S_{Hmax} < 6,691 + \sigma^T$ $6,188 < S_{Hmax} < 8,191$	N60° E?	-
GM4 (HF)	4,616	Precambrian	3,930	0.85		$5,759 + \sigma^T < S_{Hmax} < 7,790 + \sigma^T$ $7,259 < S_H < 9,290$	N67° E	90°
GM2 (HF)	4,656	Precambrian	-			-	N75° E?	90°

SOSAT requests the mean and standard deviation of the minimum principal stress S_{hmin}. Only two well-constrained values are available for the Mount Simon Sandstone. These two locations with stress measurements appear to be the zone with lowest (deeper zone – GM11B) and highest (shallower zone – GM12) Young's modulus (Figure 12). The heterogeneity in the stress field can be interpreted using Equation (3), the sonic log-derived elastic properties, and an isotropic assumption (i.e., $E_h = E_v, \nu_{hh} = \nu_{vh} = \nu_{vv}$). Equation (3) shows that higher values of the Young's modulus and lower values of the Poisson's ratio will tend to produce higher values of the horizontal stresses, all else being equal. For measurement GM12 the Young's modulus is higher and Poisson's ratio lower than those at the location of measurement GM11B. Therefore, this difference in elastic properties would lead to the expectation of a higher value of S_{hmin} at the shallower depth, despite the lower vertical stress. Using a similar rationale, these two locations represent the extreme values of the Young's modulus and Poisson's ratio within the Mount Simon Sandstone, and therefore likely represent also the extreme values of stress magnitudes.

Based on this analysis, it is reasonable to assume that the mean value for S_{hmin} is the average of the two values determined in the Mount Simon Sandstone, while the standard deviation is half the difference between them. This assumption leads to a mean of 3,020 psi (22.06 MPa) and standard deviation of 220 psi (1.52 MPa).

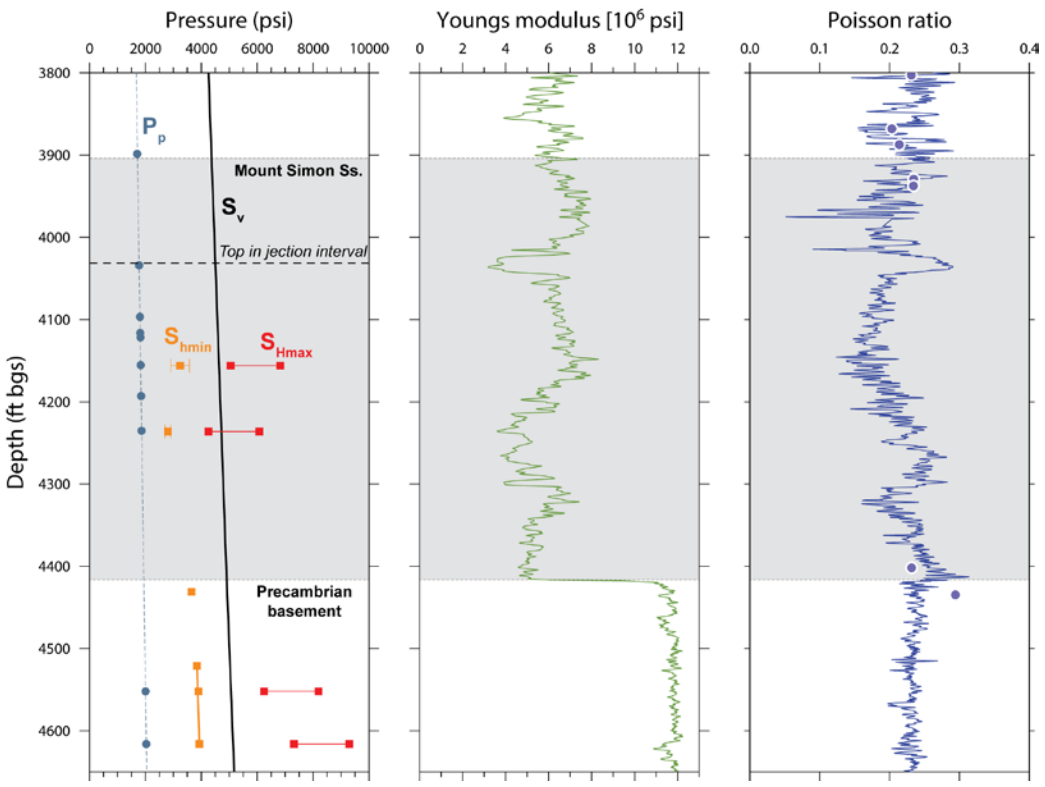

Figure 12. Left: Vertical profile of the principal stresses along with the pore pressure measurements and pore pressure gradient determined in the Mount Simon Sandstone (0.4401 psi/ft). Center and right: Young's modulus and Poisson's ratio as determined by sonic log (not calibrated).

2.3.2 Regional Observations

Figure 13 is a map of the regional stress observations from the World Stress Map database (Heidbach et al. 2016). Stress indicators of quality A, B, and C are included. Most of the regional data points are derived from borehole breakout analysis or from focal mechanisms interpretation, which provide a good constraint on principal stress directions, but not on the magnitude of the stresses (Figure 7). Based on the regional values, the anticipated maximum horizontal stress direction was expected to fall in the N45°E -N63°E direction, which is consistent with the azimuth determined by in situ stress measurements (i.e., N51±4°E in the Mount Simon Sandstone, N63±9° the Precambrian basement).

Among the stress indicators plotted in Figure 14 are the results of two hydraulic fracturing campaigns conducted in the Waterloo quartzite in Eastern Wisconsin (Haimson 1980) and in the Precambrian Granite of Northern Illinois (Haimson, Bezalel, and Doe 1983). These measurements suggest in both cases that the maximum principal stress is horizontal and the minimum horizontal stress is the minimum principal stress for depths greater than 3,280 ft (1,000 m) bgs, which is characteristic of a strike-slip faulting regime ($S_{Hmax} > S_v > S_{hmin}$). These same measurements performed in the Illinois Basin indicate that the minimum horizontal stress values may, depending on the depth, reach magnitudes close to the vertical stress values, suggesting that the fault mechanisms may change from predominantly strike-slip to reverse. SOSAT provides the possibility to consider a probability distribution function expressing the regional stress information. The calculated probability distribution is constructed using a

superposition of two logistic functions (explained by Burghardt [2018]), that allow the user to assign a weight to the different stress regimes and to set transition parameters specific to the sigmoid functions referred to as K-thrust and K-SS, that control the width of the sigmoid transitions between the three faulting regimes. The larger the value, the more abrupt the transition.

The evaluation of the regional stress data and in situ stress measurements performed at the FutureGen 2.0 site indicate that it is reasonable to assign a conservative probability of strike-slip faulting greater than a thrust faulting state, while the probability of normal faulting is approaching zero (a zero value is not a possible option in the current version of SOSAT). A weight of 15 was then assigned to the strike-slip stress state, and respective weights of 3 and 0.1 were given to the reverse and normal faulting regimes. Additional parameters specific to the sigmoid functions, referred to as K-thrust and K-SS, control the width of the sigmoid transition between the different faulting regimes. K-thrust and K-SS were respectively chosen to be 100 and 300, leading to a smooth transition between the thrust faulting and the strike-slip faulting regimes, and an abrupt transition between the strike-slip and the very low probability normal faulting state. The resulting probability distribution for g_θ is shown in Figure 14. In this plot, the parameter g_θ is a result of the specific coordinate system defined by Burghardt (2018). In this coordinate system, the thrust faulting states lie between $-1 \leq g_\theta < -\frac{\sqrt{2}}{2}$, strike-slip states lie between $-\frac{\sqrt{2}}{2} \leq g_\theta < \frac{\sqrt{2}}{2}$, and the normal faulting state lies between $\frac{\sqrt{2}}{2} \leq g_\theta < 1$.

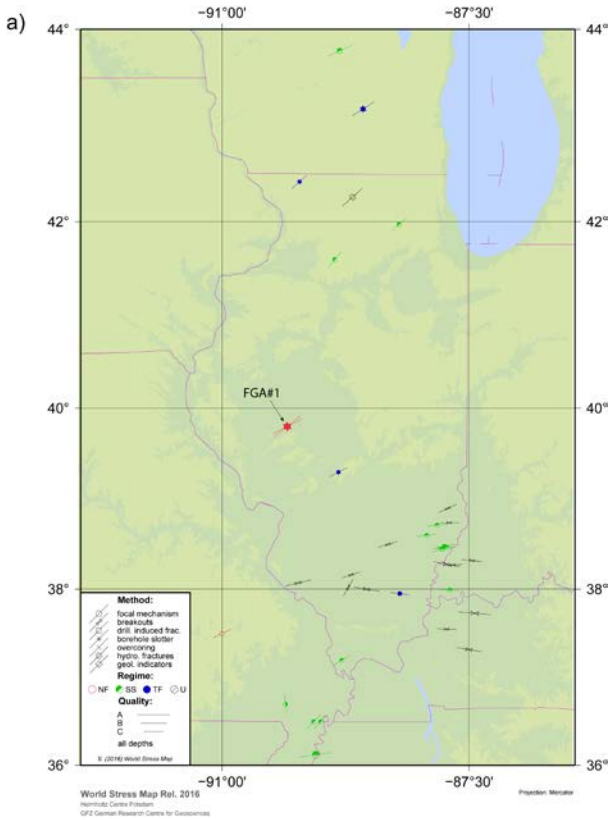

Figure 13. Plot of regional stress observation from the World Stress Map project, together with the orientation of the maximum horizontal stress measured at the FutureGen 2.0 Site (Heidbach et al 2016)

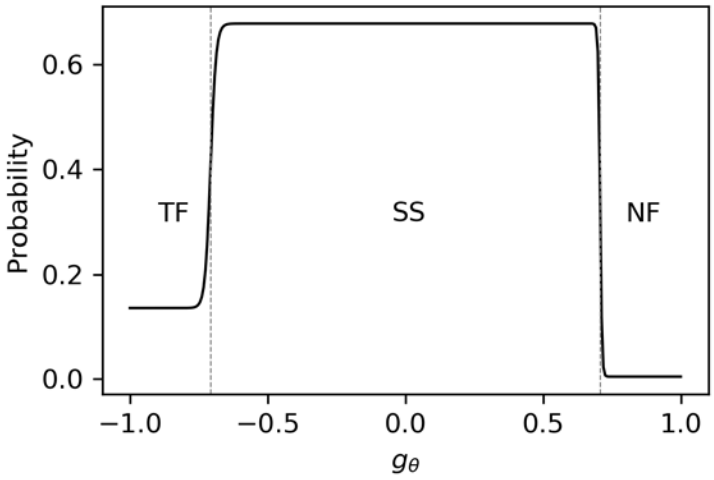

Figure 14. Plot of the probability distribution expressing the regional stress state information, with weight TF = 3, weight NF = 0.1, weight SS = 15, K-thrust = 100, and K-SS = 300.

2.3.3 Reservoir Stress Path

Subsurface activities involving fluid injection or withdrawal cause perturbations in the pore pressure. In the context of CO_2 injection in a saline aquifer, such as at the FutureGen site, the pore pressure is expected to increase locally as CO_2 progressively displaces brine in the pore space. Increasing fluid pressures may increase the likelihood of fault reactivation. Equations (3) and (4) presented earlier demonstrate that the two horizontal stresses are a combination of the Poisson effect, the distribution of the elastic properties, and the contribution of the tectonic strains. Thus, the evolution of the horizontal stresses during subsurface operations depends on several factors including the initial state prior to operations and the distribution of elastic properties. However, over the last two decades, multiple studies related to field operations have demonstrated that the stress state within a reservoir is directly coupled to pore pressure changes resulting from fluid injection or withdrawal and that horizontal stresses evolve as pore pressure builds up (Vidal-Gilbert et al. 2010; Streit and Hillis 2004; Hillis 2000). This evolution of the stress state in the reservoir associated with subsurface operations is commonly referred to as “stress path ” (Addis 1997) or “pore pressure-stress coupling” (Hillis 2001). While a stress path could be defined for each principal stress (i.e., S_v, S_{hmin}, and S_{Hmax}), a reservoir is commonly assumed to behave under uniaxial strain conditions, which means that the total vertical stress is unaffected by changes in overpressure, and that there is no change in strain in the horizontal direction. Using the transversely isotropic vertical (TIV) elastic model assumed by Burghardt (2018), the resulting stress path coefficient Γ_h is given by

$$\Gamma_h = \frac{\Delta S_h}{\Delta P_p} = \alpha_h\left(1 - \frac{C_{1133}}{C_{3333}}\right) \quad (11)$$

where

Γ_h = the horizontal stress path coefficient,
ΔS_h = the change in total horizontal stress,
α_h = the horizontal component of the Biot coefficient tensor, and
C_{1133} and C_{3333} = components of the fourth-order TIV stiffness tensor.

For an isotropic material, which is assumed for the FutureGen 2.0 case study, the two components of the TIV stiffness tensor are given by

$$C_{1133} = \frac{Ev}{(1+v)(1-2v)} \quad (12)$$

$$C_{3333} = \frac{E(1-v)}{(1+v)(1-2v)} \quad (13)$$

where E is Young's modulus and v is Poisson's ratio. The stress path coefficient Γ_h can now be expressed as

$$\Gamma_h = \frac{\Delta S_h}{\Delta P_p} = \alpha_h\left(1 - \frac{v}{1-v}\right) \quad (14)$$

The coefficient $\Gamma_h$is now dependent on two parameters only, the Biot's coeffcicient α_h and the Poisson's ratio v. Only three triaxial tests were conducted on sidewall cores from the Mount Simon Sandstone in the upper and lower section of the formation (Table 6). The Poisson's coefficient v varies from 0.232 to 0.237 which is considered a representative range of the entire injection zone for this study, although more measurements would be required to confirm this statement. The Biot's coefficient is determined to be the average of the three measurements, leading to a value of 0.71. For this range of values and based on Equation (14), the horizontal stress path coefficient Γ_h is 0.49. This value for the pore pressure-stress coupling is consistent with what has been measured in field operations in different parts of the world, where the stress path coefficient usually ranges from 0.4 to 0.7, although values as low as 0.2 and as high as 1.18 have also been measured (Hillis 2000). To be more conservative, the minimum and maximum values of the stress path coefficient used to create a uniform distribution in SOSAT are chosen to vary from 0.4 to 0.6. This means that the total horizontal stresses are expected to increase by 40 to 60% of the increase in pore pressure associated with the injection.

Table 6. Elastic properties of sidewall cores samples from the Mount Simon Formation.

Well	Formation	Depth (ft)	Young's Modulus (10^6 psi)	Young's Modulus (GPa)	Poisson's ratio	Biot's Coefficient
FGA#1	Mount Simon Ss.	3,929.1	2.8929	19.9	0.235	0.71
FGA#1	Mount Simon Ss.	3,937.4	1.5423	10.6	0.234	0.71
FGA#1	Mount Simon Ss.	4,401.9	1.4899	10.3	0.232	0.70

2.3.4 SOSAT Inputs: Summary of Stress Measurements Parameters

The site-specific parameters determined above and related to the stress measurements at the FutureGen 2.0 site are summarized in Table 7.

Table 7. Summary of the stress measurements input parameters for SOSAT.

Parameters	Values
Regional Stress Info	
Normal faulting weight	0.1
Strike-slip faulting weight	15

Parameters	Values
Thrust-faulting weight	3
Maximum possible friction coefficient	1.5 (default)
K-thrust	100
K-SS	300
Stress Measurement	
Mean of minimum principal stress measurement	3,020 psi
Standard deviation of minimum principal stress measurement	220 psi
Stress Path	
Minimum value of the stress path coefficient	0.4
Maximum value of the stress path coefficient	0.6

3.0 Geomechanical Risk Assessment at the FutureGen 2.0 Site: Results

All required parameters were set in the four tabs of the SOSAT user interface (Figure 15). The analysis routine was launched and provided two distinct plots and their associated data: the posterior distribution plot (Figure 16) and the fault activation probability plot (Figure 17). The information provided by these SOSAT outputs can then be used for assessing the geomechanical risk at the carbon storage site.

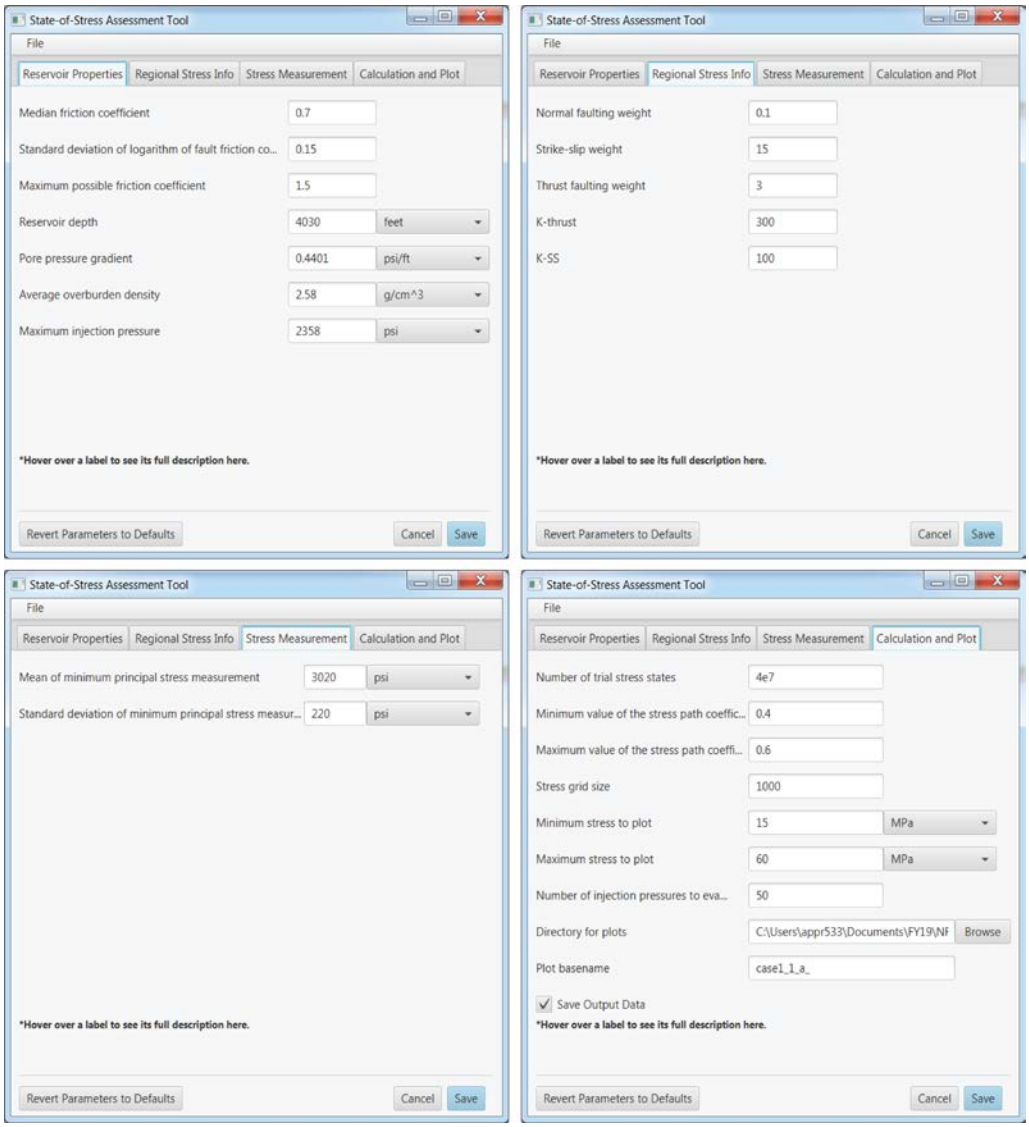

Figure 15. SOSAT user interface with parameters used for assessing the risk of fault reactivation and hydraulic fracturing at the FutureGen 2.0 site.

3.1 Risk of Induced Shear Failure

3.1.1 Posterior Stress Distribution at Elevated Pore Pressure

The posterior stress distribution presented in Figure 16 shows that the minimum horizontal stress is well constrained by the geomechanical tests performed in the Mount Simon Sandstone. The results also demonstrate the relatively high degree of uncertainty on the magnitude of the maximum horizontal stress S_{Hmax}; possible values range from about 32 MPa to 53 MPa. The total probability of induced shear failure as a function of pore pressure change is determined in SOSAT and plotted in Figure 17. This plot shows that the probability that the Mount Simon reservoir was initially critically stressed is relatively high as indicated by the value of 25%. When the pore pressure increases to 16.2 MPa (2,320 psi), determined to be the maximum allowable pressure permitted under the UIC Class VI regulation of the FutureGen 2.0 project, the risk of shear failure approaches a probability of 43%. These relatively high probabilities reflect the current state of information about the geomechanical conditions in this part of the Illinois Basin. Both of these values are caused primarily by a lack of characterization of the maximum horizontal stress. Further characterization of the S_{Hmax} could significantly reduce this uncertainty and may lead to a determination that the site is not in fact critically stressed. For future operations in this basin this is should be a high characterization priority because it could significantly lower the risk of operations.

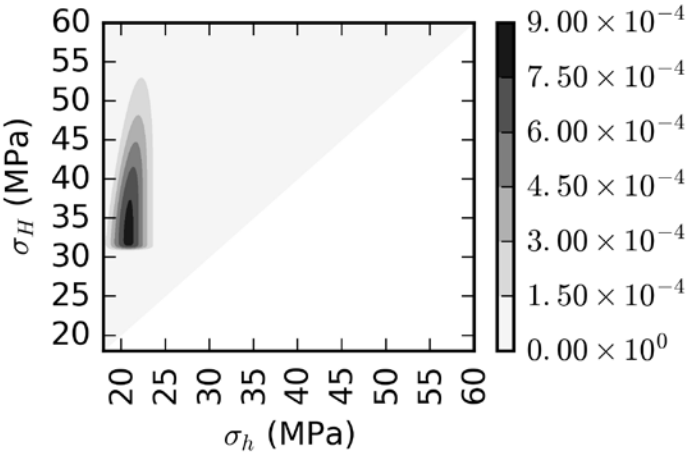

Figure 16. Posterior stress distribution plot at the FutureGen 2.0 site.

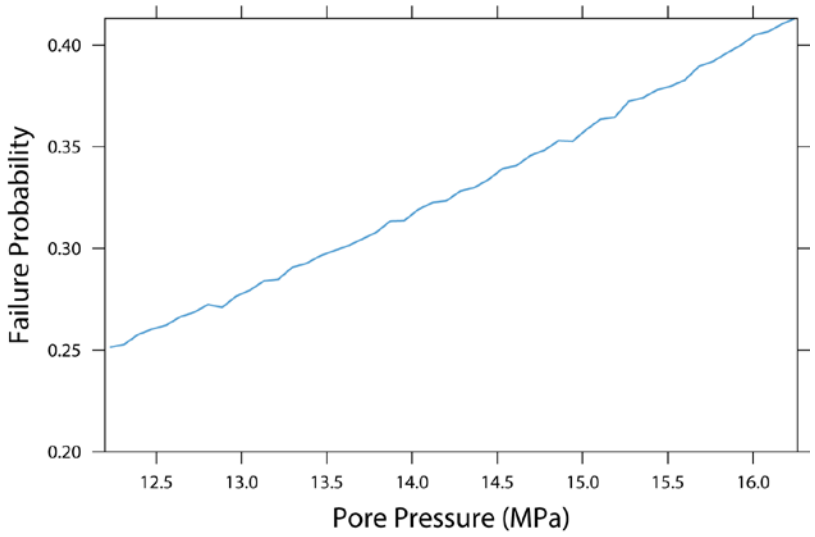

Figure 17. Probability of inducing shear failure on a critically oriented fault plane for a given pore pressure at the FutureGen 2.0 site.

3.1.2 Effect of Parameters on Risk of Induced Shear Failure

The effects of moderate changes in the input parameters were evaluated by varying their respective probability distributions. A set of four cases was first tested. In the four scenarios, the probability distribution for the regional stress state remained identical to the base case presented above (i.e., strike-slip faulting regime with a limited likelihood of a thrust faulting stress state). Only the probability distribution of the friction coefficient (case 1.2.a), the range of stress path values (case 1.1.b), or both (case 1.2.b) were modified. The median of the friction coefficient was considered to be 0.6 or 0.7, with the standard deviation remaining at 0.15. The minimum and maximum values for the stress path coefficient were either chosen to range from 0.4 to 0.6, or from 0.4 to 0.8. The results of these changes were plotted in Figure 18, along with the base case scenario labeled as “case 1.1.a.”

The effects of similar changes on the same parameters were also evaluated and are plotted in Figure 19; only the probability distribution of the regional stress state differs from the results presented in Figure 18. A probability distribution assuming a pure strike-slip stress state is considered for this set of scenarios.

These results show first that the probability distribution chosen for the regional state stress (i.e., either strike-slip faulting regime with limited probability for thrust faulting, or pure strike-slip regime) has little or no effect on the posterior stress distribution.

Decreasing the coefficient of friction increases the probability of inducing shear failure. For instance, while there is a 25% probability that the Mount Simon reservoir was critically stressed before the start of the injection (Figure 18, case 1.1.a), this probability increases to 28% with a coefficient of friction of 0.6 (Figure 18, case 1.2.a).

Similarly, the range of values determined for the stress path coefficient have a significant effect on the probability of fault activation. A lower range of values for the stress path results in a higher probability of fault activation when the pore pressure increases (cases 1.1.a and 1.1.b.).

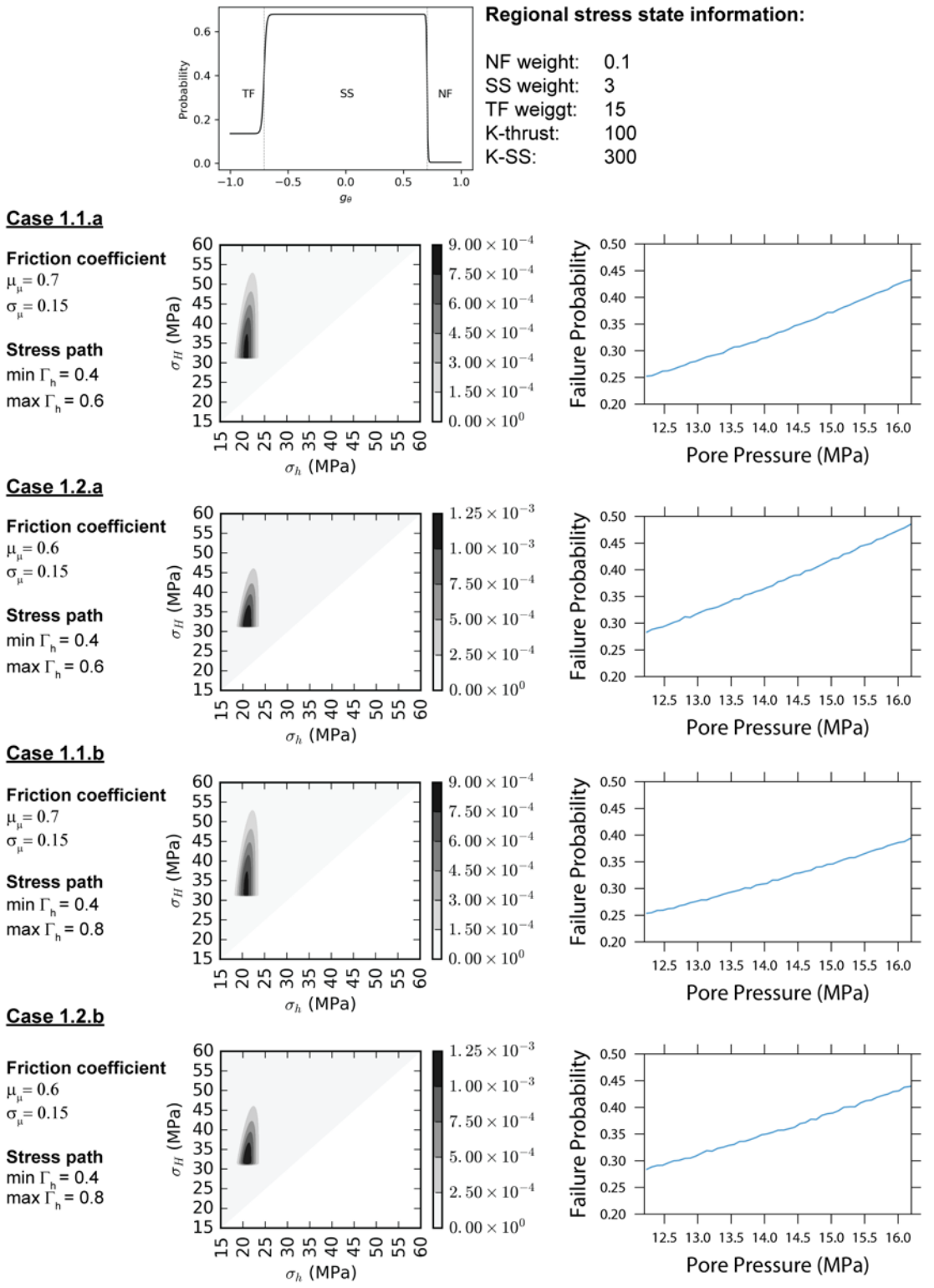

Figure 18. Effect of input parameters on the risk of induced shear stress (strike-slip faulting regime with a small probability of thrust faulting).

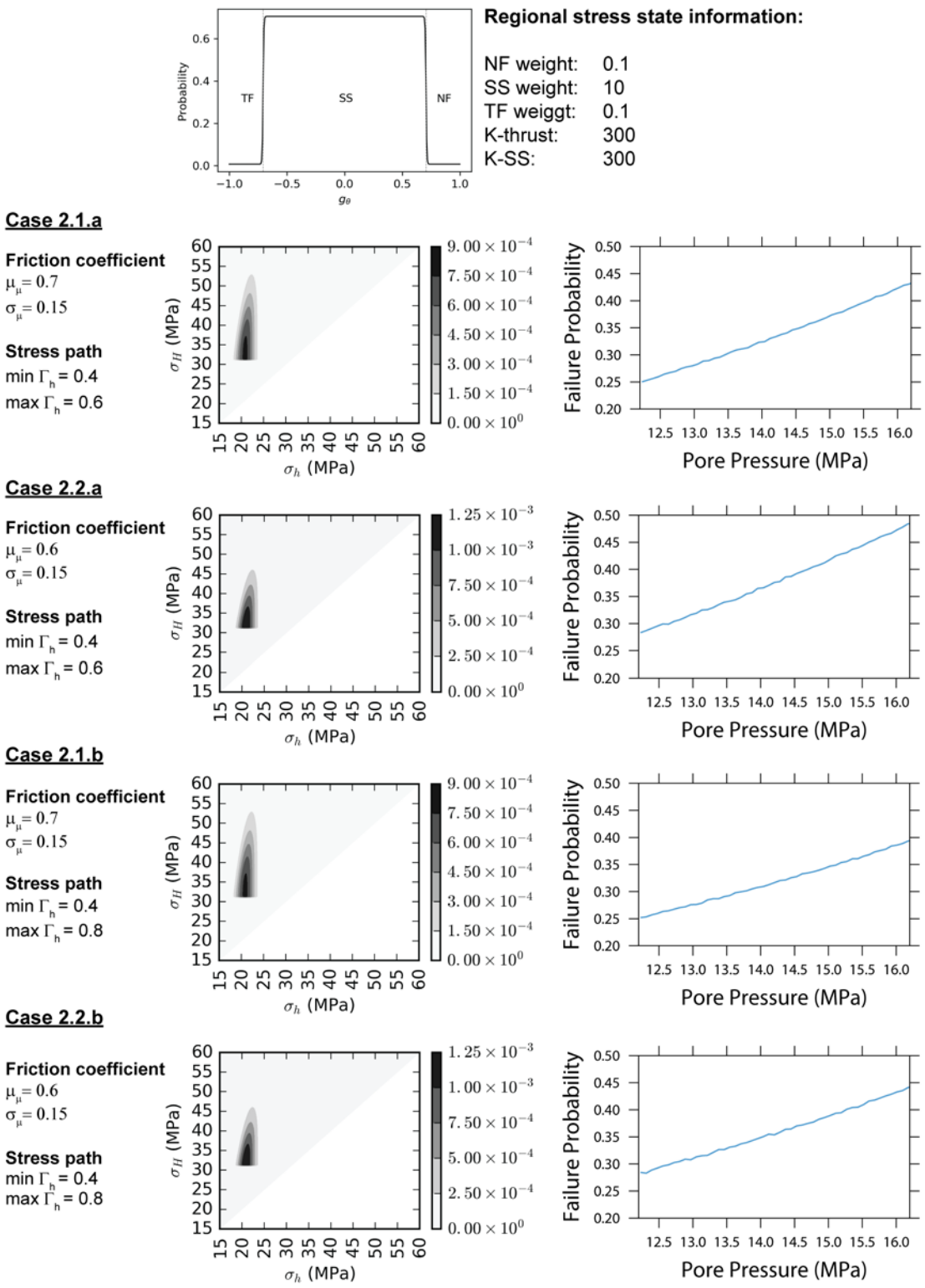

Figure 19. Effect of input parameters on the risk of induced shear stress (pure strike-slip faulting regime).

3.2 Risk of Unintentional Hydraulic Fracturing

The risk of unintentional hydraulic fracturing was also evaluated. To prevent the initiation of hydraulic fractures, the injection pressure must remain smaller than the minimum principal stress. Three scenarios were evaluated, assuming that either a 1%, 5%, or 10% risk of fracturing was acceptable. Based on the cumulative probability distribution obtained from the posterior stress distribution calculated with SOSAT (see Section 3.1), the maximum allowable pressure under initial reservoir conditions was obtained for the three scenarios (Figure 20). Under the 1% probability threshold (i.e., 99% of the possible stress states would not produce a hydraulic fracture), an injection pressure of 18.19 MPa was found, whereas 19.15 MPa and 19.65 MPa were respectively determined for a 5% or 10% risk of fracturing.

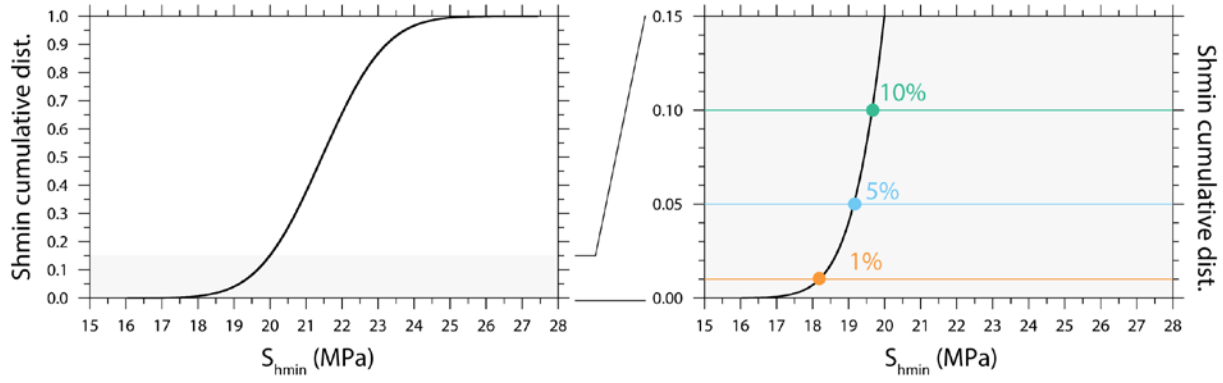

Figure 20. (a) Cumulative distribution of the minimum horizontal stress (Shmin) as determined by SOSAT (see Section 3.1) and (b) the determination of the maximum allowable injection pressure under initial reservoir conditions corresponding to a 1%, 5%, and 10% risk of hydraulic fracturing.

Using the value of the stress path Γ_h coefficient determined in Section 2.3.3, the maximum safe injection pressure is expected to increase by 49% of the average pore pressure increase. Figure 21 presents a plot of the maximum allowable injection pressure that would result in either a 1%, 5%, or 10% risk of hydraulic fracturing as a function of average reservoir pore pressure. This plot shows that once the pore pressure builds up in the reservoir, the injection pressure can be increased while maintaining the same probability of inducing hydraulic fracturing. This increase in the same injection pressure does not apply to the risk of induced seismicity.

While two types of geomechanical risks are considered in this study (i.e., shear failure and hydraulic fracturing), the interpretation of the results delivered by SOSAT clearly demonstrates that, for the current state of knowledge at the FutureGen 2.0 site, the risk of induced shear failure during injection operations is higher than the risk of induced hydraulic fracturing. This is due to the relatively well characterized value of the minimum principal stress.

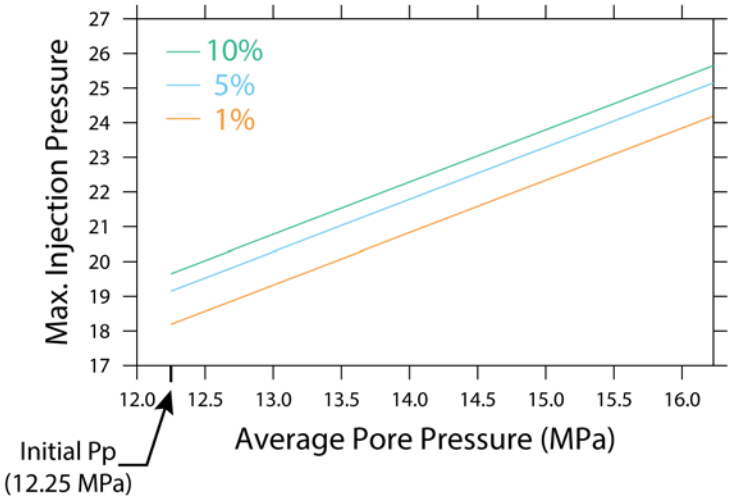

Figure 21. Injection pressure that would produce a 1% (orange), 5% (blue), and 10% (green) probability of hydraulic fracturing as a function of reservoir pore pressure.

4.0 Conclusions

This study evaluated the geomechanical risk associated with hypothetical CO_2 injection at the FutureGen 2.0 site, using SOSAT. SOSAT is a user-friendly tool used to estimate the stress state at a given depth in the subsurface. The stress estimation is conducted using a modified version of two commonly used stress estimation methods—the stress polygon approach and the 1D tectonic-elastic approach—to account for uncertainty in the input parameters.

The input parameters required in SOSAT include initial reservoir conditions, such as pore pressure, depth, and pressure of planned injection, as well as optional information about the regional stress state and stress measurement data. Most of the data required in SOSAT were available at the FutureGen 2.0 site thanks to the extensive characterization conducted in support of the applications for the four UIC Class VI permits. The data required in SOSAT for the geomechnical assessment of the FutureGen 2.0 site were identified, and the methodology proposed in SOSAT was followed to evaluate the probability of reactivating critically oriented faults or potentially creating new hydraulic fractures in the reservoir. The results of the geomechnical analysis performed in SOSAT led to the following conclusions:

1. The probability distribution of the state of stress indicates significant uncertainties in the magnitude of the maximum horizontal stress S_{Hmax}, while the minimum horizontal stress Shmin is well constrained by the stress measurements conducted during the characterization efforts at the storage site. This uncertainty in the magnitude of S_{Hmax} is a common challenge and has significant implications for geomechanical risk at sites like FutureGen 2.0 where a strike-slip tectonic regime exists.
2. The probability that the Mount Simon reservoir was initially critically stressed is relatively high—25%. When the pore pressure increases to the maximum allowable pressure permitted under the UIC Class VI regulation of the FutureGen 2.0 project, the risk of shear failure approaches a probability of 43%. These relatively high probabilities reflect the current state of information about the geomechanical conditions in this part of the Illinois Basin and in particular the lack of characterization of the maximum horizontal stress. For future operations in this basin this should be a high characterization priority because it could significantly lower the risk of operations.
3. The shear failure risk is the dominant geomechnical risk compared to the risk of unintentional hydraulic fracturing. This is largely due to the well-constrained value of the minimum principal stress.

The risk of shear failure in SOSAT is based on a very conservative approach assuming that critically oriented faults exist in the subsurface. While no faults have been formally identified at the FutureGen 2.0 site, the results obtained with SOSAT using the FutureGen 2.0 data set highlight the importance of integrating uncertainties in critical parameters to quantify geomechanical risks in a defensible way.

In the life cycle of a CCS project, SOSAT could be used from site-screening to the end of the injection operations. Applying SOSAT in the initial phases of a CCS project could help defining critical data that would reduce geomechanical uncertainties at a given site. Additionally, SOSAT could also be an important tool in the permitting phase when informed decisions must be made regarding critical operational parameters (i.e., maximum injection pressure) that condition the injection operations for years. During injection operations, SOSAT could be used in combination with monitoring observations data to help understanding the overall geomechanical behavior of the storage complex.

5.0 References

Addis, M. A. 1997. "The Stress-Depletion Response Of Reservoirs." SPE Annual Technical Conference and Exhibition, San Antonio, Texas, 1997/1/1/.

Anderson, E.M. 1951. "The Dynamics of faulting and dyke formation with applications to Britain." *Edinburgh: Olivier and Boyd*.

Burghardt, J. 2018. "Geomechanical Risk Assessment for Subsurface Fluid Disposal Operations." *Rock Mechanics and Rock Engineering* 51 (7):2265-2288. doi: 10.1007/s00603-018-1409-1.

Cornet, F. H. 2014. Results from the in-situ stress characterization program; phase 1: geomechnical tests conducted in teh FutureGen stratigraphic well (FGA#1). Geostress

Cornet, François H., and Thomas Röckel. 2012. "Vertical stress profiles and the significance of “stress decoupling”." *Tectonophysics* 581:193-205. doi: https://doi.org/10.1016/j.tecto.2012.01.020.

Gilmore, Tyler, Alain Bonneville, Charlotte Sullivan, Mark Kelley, Delphine Appriou, Vince Vermeul, Signe White, Fred Zhang, Bruce Bjornstad, Francois Cornet, Jacqueline Gerst, Neeraj Gupta, Gretchen Hund, Jake Horner, George Last, Dave Lanigan, Mart Oostrom, Caitlin McNeil, Mark Moody, Mark Rockhold, Mike Elliott, Frank Spane, Chris Strickland, Lucy Swartz, Paul Thorne, Christopher Brown, Jeffrey Hoffmann, and Kenneth Humphreys. 2016. "Characterization and design of the FutureGen 2.0 carbon storage site." *International Journal of Greenhouse Gas Control* 53:1-10. doi: http://dx.doi.org/10.1016/j.ijggc.2016.07.022.

Haimson, B. C., and F. H. Cornet. 2003. "ISRM Suggested Methods for rock stress estimation—Part 3: hydraulic fracturing (HF) and/or hydraulic testing of pre-existing fractures (HTPF)." *International Journal of Rock Mechanics and Mining Sciences* 40 (7–8):1011-1020. doi: 10.1016/j.ijrmms.2003.08.002.

Haimson, Bezalel C., and Thomas W. Doe. 1983. "State of stress, permeability, and fractures in the Precambrian granite of northern Illinois." *Journal of Geophysical Research: Solid Earth* 88 (B9):7355-7371. doi: 10.1029/JB088iB09p07355.

Heidbach, Oliver;, Mojtaba; Rajabi, Karsten; Reiter, and Moritz Ziegler. 2016. "The World Stress Map Database Release 2016." GFZ Data Services. .

Hillis, Richard. 2000. "Pore Pressure/Stress Coupling and its Implications for Seismicity." *Exploration Geophysics* 31 (1-2):448-454. doi: 10.1071/EG00448.

Hillis, Richard R. 2001. "Coupled changes in pore pressure and stress in oil fields and sedimentary basins." *Petroleum Geoscience* 7 (4):419-425. doi: 10.1144/petgeo.7.4.419.

Jaeger, J. C., and N. G. W. Cook. 1979. *Fundamentals of Rock Mechanics, Third ed.* London: Chapman and Hall.

Langenbruch, Cornelius, and Mark D. Zoback. 2016. "How will induced seismicity in Oklahoma respond to decreased saltwater injection rates?" *Science Advances* 2 (11):e1601542. doi: 10.1126/sciadv.1601542.

Nicol, A., R. Carne, M. Gerstenberger, and A. Christophersen. 2011. "Induced seismicity and its implications for CO2 storage risk." *Energy Procedia* 4:3699-3706. doi: https://doi.org/10.1016/j.egypro.2011.02.302.

Streit, Jürgen E., and Richard R. Hillis. 2004. "Estimating fault stability and sustainable fluid pressures for underground storage of CO2 in porous rock." *Energy* 29 (9):1445-1456. doi: https://doi.org/10.1016/j.energy.2004.03.078.

Thiercelin, M. J., and R. A. Plumb. 1994. "A Core-Based Prediction of Lithologic Stress Contrasts in East Texas Formations." *SPE Formation Evaluation* 9 (04):251-258. doi: 10.2118/21847-PA.

Vidal-Gilbert, Sandrine, Eric Tenthorey, Dave Dewhurst, Jonathan Ennis-King, Peter Van Ruth, and Richard Hillis. 2010. "Geomechanical analysis of the Naylor Field, Otway Basin, Australia: Implications for CO2 injection and storage." *International Journal of Greenhouse Gas Control* 4 (5):827-839. doi: 10.1016/j.ijggc.2010.06.001.

Walsh, F. Rall, and Mark D. Zoback. 2015. *Oklahoma's recent earthquakes and saltwater disposal*. Vol. 1. Journal Article.

White, Joshua A., and William Foxall. 2016. "Assessing induced seismicity risk at CO2 storage projects: Recent progress and remaining challenges." *International Journal of Greenhouse Gas Control* 49:413-424. doi: https://doi.org/10.1016/j.ijggc.2016.03.021.

Zoback, M. D., C. A. Barton, M. Brudy, D. A. Castillo, T. Finkbeiner, B. R. Grollimund, D. B. Moos, P. Peska, C. D. Ward, and D. J. Wiprut. 2003. "Determination of stress orientation and magnitude in deep wells." *International Journal of Rock Mechanics and Mining Sciences* 40 (7–8):1049-1076. doi: 10.1016/j.ijrmms.2003.07.001.

Zoback, Mark D., and Steven M. Gorelick. 2012. "Earthquake triggering and large-scale geologic storage of carbon dioxide." *Proceedings of the National Academy of Sciences* 109 (26):10164-10168. doi: 10.1073/pnas.1202473109.

.

PNNL-28657

Pacific Northwest National Laboratory

902 Battelle Boulevard
P.O. Box 999
Richland, WA 99354
1-888-375-PNNL (7665)

www.pnnl.gov